

Tensorial solution of the Poisson equation and the dark matter amount and distribution of UGC 8490 and UGC 9753

P. Repetto^{1*}

¹*Via Gallaretta 42, Castelletto d'Orba, Alessandria, C.P. I-15060, Italia*

Accepted XXX. Received YYY; in original form ZZZ

ABSTRACT

In the first part of this article we expand three fundamental aspects of the methodology connected to the determination of a relation among the spatial density and the gravitational potential that can be specialised to distinct mass density agglomerations. As a consequence, we obtain general relations for the diagonal entries of a square symmetric matrix without zeros, we provide an expression of the gravitational potential, suitable, to represent several different mass density configurations, and we determine relations for the semi-axes of a triaxial spheroidal mass distribution, as a function of the spheroid mass density, volume density and radius. In the second part of this manuscript, we employ the tools developed in the first part, to analyse the mass density content and the inner and global structure of the dark matter haloes of UGC 8490 and UGC 9753, through the fits to the dark matter rotation curves of the two galaxies, assuming a triaxial spheroidal dark matter mass configuration. We employ the Navarro Frenk and White, Burkert, DiCintio, Einasto and Stadel dark matter models, and we obtain that both a cored Burkert and cuspy DiCintio and Navarro Frenk and White inward dark matter distributions could represent equally well the observed data, furthermore we determine an oblate spheroidal dark matter mass density configuration for UGC 8490 and UGC 9753. The latter outcome is confirmed by the estimation of the gravitational torques exerted by the dark matter halo of each analysed galaxy, on the corresponding baryonic components.

Key words: galaxies: irregular – galaxies: kinematics and dynamics – galaxies: dwarf – galaxies: individual: UGC 8490 and UGC 9753

1 INTRODUCTION

The global quantity and configuration of mass in galaxies represents an interesting astrophysical problem of many facets, that was first addressed in the period among the forties and the sixties, by several authors, in an attempt to determine, on the one hand, an approximate value of the whole mass of the studied galactic systems, and, on the other hand, the more adequate volumetric aggregation of the corresponding galactic masses up to a certain radial extent, defined by the utmost radius of the observed rotation curves (RCs), of each analysed object. In that regard, the most noteworthy contributions, are those of [Burbidge et al. \(1959\)](#) and [Brandt \(1960\)](#), that determine the total mass distribution of some nearby galaxies, considering that the

observable part of those galaxies could be approximated by a set of concentric oblate spheroids.

The discrepancy among the total mass and the luminous mass of a certain number of local galaxies was determined by some authors, including [Hubble \(1929\)](#), [Babcock \(1939\)](#), [Wyse & Mayall \(1942\)](#), through a kinematic and photometric analysis, together with a study of the RCs of the selected galaxies, to obtain an estimation of the total dynamic mass of the analysed galactic systems. The first studies, regardless of their fundamental importance, are unable to establish unambiguously the correct value of the mass-to-light (M/L) ratios of the analysed objects, principally due to the large uncertainties associated to the spectroscopic and photometric measurements necessary to obtain an estimation of the luminosity and total mass of the selected galaxies.

The determination of more robust M/L ratios, together with other important results, were accomplished at the end of the seventies, as a consequence of the rapid advancement

* E-mail: prsatch6@gmail.com

of the spectroscopic and photometric observational techniques utilised for the data collection, as well as, the improvement of the procedures for the reduction and analysis of the data. Some of the more prominent works that illustrate the fundamental changes delineated above, are outlined in the following. [Rubin et al. \(1978\)](#) studied a sample of 10 high surface brightness massive spirals, of morphological types from Sa to Sc, to ascertain, among other findings, an average optical blue band M/L ratio of 3.5. In a similar work, [Rubin et al. \(1985\)](#), using optical luminosities in the blue band, determine, jointly with other outcomes, the mean values of the M/L ratios, of a sample of 54 spiral galaxies to be 6.2, 4.2 and 2.6, for the morphological types Sa, Sb, Sc, respectively, within the isophotal radius 25. [Burstein & Rubin \(1985\)](#), and [Burstein et al. \(1986\)](#) analysed a total sample of 80 RCs of Sa, Sb and Sc galaxies, determining the whole gravitating mass of these systems. The quoted articles, together with several other works (e.g. [Kent 1987](#); [Persic & Salucci 1990](#); [Forbes 1992](#); [Persic et al. 1996](#); [Takamiya & Sofue 2000](#)), established stronger observational evidences, on galactic scale, of the existence of a non observable mass component, specifically the dark matter (DM), whose total amount and related kinematical and dynamical effects could eventually affect the evolution of any other galactic constituent, as well as of the entire galaxy.

From the end of the nineties to the present time, the majority of the observational efforts have been directed to improve the quality of the observed RCs, ameliorating the spatial and spectral resolution of the photometric and spectroscopic data, to determine much more reliable constraints on the estimated baryonic and DM masses, and to establish the actual total mass distribution of galaxies of different morphological types, based on more advanced and robust methods of data reduction and analysis. In particular the principal interests are devoted to the study of the inner mass configuration of dwarf galaxies of low surface brightness, where it is supposed that DM rules the entire dynamics, and for that reason its gravitational effects on the other galactic components, could be studied in a more precise and direct manner (e.g. [Blais-Ouellette et al. 2001, 2004](#); [Spano et al. 2008](#); [de Blok et al. 2008](#); [Kuzio de Naray et al. 2009](#)). The contrast among the theoretical predictions of an infinite amount of mass in the internal regions of galaxies and the observational detections of a finite DM inner mass distribution, represents the cuspy/core issue, addressed for several years by many authors, from a theoretic and observational perspective, and that still constitutes an unsettled matter of large study and debate (e.g. [Salucci et al. 2010](#); [Plana et al. 2010](#); [Karukes et al. 2015](#); [Allaert et al. 2017](#); [Korsaga et al. 2018](#); [de Blok 2018](#)).

The current manuscript is dedicated to the creation of some general tool to analyse the dynamics and kinematics of various 3D mass distributions, and, as an application, of the novel developed technique, we perform the fits to the H α and HI DM RCs of UGC 8490 and UGC 9753, to obtain the total and DM mass of both galaxies, together with its global spatial configuration. In the following we proceed illustrating the principal matters studied in this article.

In the first part of the present work we propose a generalisation of some of the most important aspects of the methodology introduced in [Repetto et al. \(2018\)](#) (RP18), in particular, we diagonalize a square symmetric matrix with

three columns and rows (3SSM) without null elements, we determine an integral solution of the Poisson equation appropriate to describe the gravitational potential of several different 3D mass density distributions, and we find out the relations of the semi-axes of a hypothetical DM triaxial spheroid, as parametric ratios of the DM masses, scale radii and the corresponding volume densities. The second part of the current paper examines the potentiality of the extension of the approach of RP18, performed in the first part of the current study, investigating the DM and total mass content of UGC 8490 and UGC 9753, hypothesising that the DM haloes of both galaxies could be appropriately described through a triaxial spheroidal mass arrangement of non uniform volume density. In particular we employ the DM density profiles of Navarro, Frenk and White, [Navarro et al. \(1996\)](#) (NFW), Burkert, [Burkert \(1995\)](#) (BKT), Di Cintio, [Di Cintio et al. \(2014\)](#) (DCN), Einasto, [Einasto \(1965\)](#) (EIN) and Stadel, [Stadel et al. \(2009\)](#) (STD). We determine that the inner DM mass distribution of UGC 8490 and UGC 9753 analysed through the H α and HI DM RCs are well represented by the following DM velocity profiles: the cored BKT and the cuspy DCN, for the H α DM RC of UGC 8490 and UGC 9753, separately, and the cuspy DCN and NFW, for the HI DM RC of UGC 8490 and UGC 9753, respectively. The overall DM distribution of the two galaxies analysed in this work is well described by a flattened DM mass density configuration. It is important to note that in this manuscript we do not attempt to address the cuspy/core discrepancy, given the insufficient number of RCs analysed and the non adequate spatial resolution of the HI DM RCs, instead we assess the potentiality of the determined integral solution of the Poisson equation, by means of the application presented in section (6).

The content of the current manuscript is the following: in Section (2), and in the Appendix (A) we present some relations to transform a non orthogonal system of curvilinear coordinates to an orthogonal one, in Section (3) and in the Addendum (B) we determine a general integral solution of the Poisson equation, in Section (4) and in the Supplement (D) we determine the semi-axes relations for a triaxial spheroidal DM configuration, in Section (5) and Addendum (C) we specialise the Poisson integral solution to a triaxial spheroidal mass distribution and characterise the rotation through an exact formula in the corresponding equatorial plane, in Section (6) and the relative subsections we apply the previous results to the determination of the amount and distribution of the DM mass of UGC 8490 and UGC 9753, in Section (7) we determine the values of the semi-axes of the hypothesised DM triaxial spheroid by means of the gravitational torques method, we present two mock data trials, to appraise the robustness of the conceived methodology, and a comparison with other studies, in Section (8) is presented a discussion of the principal attainments of the current article, whereas the conclusions are detailed in Section (9).

2 EXTENSION OF THE METHODS OF RP18

In the next three sections, that constitute the first part of this work, we present a generalisation of the essential steps that are inherent to the methodology developed in RP18,

in addition we provide some relations to derive an orthogonal curvilinear coordinates system from a non orthogonal one, and we determine the semi-axes of a triaxial spheroidal distribution of matter as a function of the spheroidal mass density, volume density and radius. Specifically, the procedural extension is concerned with a general solution of the Poisson equation applicable to many different mass configurations, the diagonalization of a 3SSM with non null elements, and the determination of three expressions for the semi-axes of the supposed triaxial spheroidal mass distribution. The introduced methodology expansion is appropriate for 3D mass configurations, and the subsequent astrophysical application, that represents the second part of this article, takes advantage of that extension.

2.1 Diagonalization of a 3SSM without null entries

In this section we compute the diagonal elements of a 3SSM that has all entries different from zero. We solve the system of the three equations derived through the equalities between the coefficients of the characteristic polynomial of the 3×3 diagonal matrix and the characteristic polynomial of the 3SSM without null elements. The most important details about the relevant equations and the calculations accomplished, are given in Appendix (A), whereas the nine solutions, are reported below. We indicate the 3SSM through the symbol M_{ml} , its corresponding elements with small capitals v letters, and the entries of the diagonal matrix with capital v letters. The nine relations, that transform a non orthogonal system of curvilinear coordinates to an orthogonal one are expressed, in compact form, through the following equations:

$$V_{ii}^{(+,-)} = \left\{ \left[\frac{\text{Tr}(M_{ml}) \pm \Delta^{(i)}}{2} \right] \right\} \quad (2.1)$$

$$V_{kk}^{(+,-)} = \frac{1}{2} \left\{ V_{ii}^{(-,+)} \pm \Delta_1^{(i)} \right\} \quad (2.2)$$

$$V_{jj}^{(-,+)} = \frac{1}{2} \left\{ V_{ii}^{(-,+)} \mp \Delta_1^{(i)} \right\} \quad (2.3)$$

where the quantities $\Delta^{(i)}$ and $\Delta_1^{(i)}$ are defined according to the ensuing relations:

$$\begin{aligned} \Delta^{(i)} &= \sqrt{[v_{kk} + v_{jj} - v_{ii}]^2 + 4[v_{ik}^2 + v_{ij}^2]} \\ \Delta_1^{(i)} &= \sqrt{[V_{ii}^{(-,+)}]^2 - 4[v_{kk}v_{jj} - v_{kj}^2]} \end{aligned} \quad (2.4)$$

The indices i, k, j satisfy the condition $i \neq k \neq j$ and range from 1 to 3, through all possible permutations. Particular instances of the solutions provided above, are determined whenever pairs of non diagonal matrix elements are zero. The solution of RP18 can be obtained, for instance, setting $i = 2, k = 3, j = 1$, $v_{12} = v_{23} = 0$ and $v_{13} \neq 0$. Other specific solutions are determined interchanging 13 with 12 and 13 with 23, and considering $i = 3, k = 2, j = 1$, and $i = 1, k = 3, j = 2$, respectively. The solutions above constitute a set of fundamental transformations among non orthogonal and orthogonal systems of curvilinear coordinates. In the present manuscript we employ equation (2.1), (2.2)

and (2.3) to orthogonalise the non orthogonal curvilinear system of coordinates utilised to address the particular issue analysed in the subsequent part of this work.

3 INTEGRAL SOLUTION OF THE POISSON EQUATION

In the present section we determine an integral solution of the Poisson equation, to obtain an expression of the gravitational potential, appropriate to describe several different mass density configurations. In appendix (B) we provide the complete details of that derivation. The gravitational potential formula, established in this work, expresses the radial derivative of the 3D gravitational potential as an integral function of the diagonal entries of the metric tensor matrix, and therefore it is supposed that the spatial density points can be properly described by a system of Cartesian or curvilinear coordinates that is orthogonal, or alternatively, that can be reduced to orthogonal form, through matrix diagonalization. It is evident from addendum (B), that we actually obtain the gradient of the 3D gravitational potential, not only its radial derivative, however we concentrate on that latter quantity solely for the purpose of the analysis performed in this article. The radial partial derivative of the gravitational potential can be expressed in the following manner:

$$\begin{aligned} \frac{\partial \phi_1(u_1, u_2, u_3)}{\partial u_1} &= \\ &= \sqrt{\frac{V_{11}}{V_{22}V_{33}}} \left[4\pi G \int_0^{u_1} \rho_1(v_1, v_2, v_3) \sqrt{V} dv_1 + C_1 \right]. \end{aligned} \quad (3.1)$$

where G is the Newtonian constant of gravitation. The volume density is represented by the quantity $\rho_1(u_1, u_2, u_3)$, and a non specific system of curvilinear coordinates (u_1, u_2, u_3) defines the loci of the spatial density points. The solution (3.1), encompasses both the Laplace and Poisson equations, i.e. the homogeneous and non homogeneous differential equation. The quantity V corresponds to the determinant of the diagonal metric tensor matrix, and the constant C_1 have to be expressed in units of $\text{kpc km}^2 \text{s}^{-2}$. The particular problem studied in this manuscript requires the application of the solution (3.1) to a spheroidal system of curvilinear coordinates and, in addition, for the specific objective of this research, we have to omit the homogeneous part of that solution.

4 TRIAXIAL SPHEROID SEMI-AXES EXPRESSIONS

This section illustrates the relations obtained for the semi-axes of a triaxial spheroidal mass density configuration, that can be parametrized through the resultant DM fit parameters, such as, for instance, the DM halo mass and scale radius, and the corresponding DM halo volume density. In the subsequent part of the present section we report the relevant equations, whereas the complete derivation of the semi-axes parametrizations is left to appendix (D). We determine, as a first step, the products of the semi-axes, i.e. the quantities $a_1 a_2$, $a_1 a_3$ and $a_2 a_3$, considering the relations of the 3D total spheroidal mass density, and the related 2D surface mass

densities on the equatorial ellipse, and the other two perpendicular ellipses, within the triaxial spheroid. Once obtained the semi-axes products, we determine the semi-axes a_1 , a_2 and a_3 , for a triaxial spheroidal mass density distribution, and in the case where the equatorial ellipse of the analysed spheroidal density aggregation is a circle. The equations of the semi-axes in the case $a_1 \neq a_2 \neq a_3$ are the following:

$$\begin{aligned} a_1 &= \left[\frac{1}{4\pi} \left(\frac{I_{1d}}{I_{1M}} \right) \left(\frac{I_{2M}}{I_{2d}} \right) \left(\frac{I_{3M}}{I_{3d}} \right) \right]^{\frac{1}{2}} \\ a_2 &= \left[\frac{1}{4\pi} \left(\frac{I_{1M}}{I_{1d}} \right) \left(\frac{I_{3M}}{I_{3d}} \right) \left(\frac{I_{2d}}{I_{2M}} \right) \right]^{\frac{1}{2}} \\ a_3 &= \left[\frac{1}{4\pi} \left(\frac{I_{1M}}{I_{1d}} \right) \left(\frac{I_{2M}}{I_{2d}} \right) \left(\frac{I_{3d}}{I_{3M}} \right) \right]^{\frac{1}{2}} \end{aligned} \quad (4.1)$$

where the quotients $\frac{I_{1d}}{I_{1M}}$ and $\frac{I_{2M}}{I_{2d}}$, can be expressed as constant ratios of the resultants DM halo masses and scale radii, and the correspondent volume densities, and their reciprocal, respectively, as delineated in the addendum (D). The semi-axes relations for the instance $a_1 = a_2 \neq a_3$, are given through the ensuing formulas:

$$\begin{aligned} a_1 = a_2 &= \left[\frac{1}{4\pi} \left(\frac{I_{3M}}{I_{3d}} \right) \right]^{\frac{1}{2}} \quad a_3 = \left[\frac{1}{4\pi} \left(\frac{I_{3d}}{I_{3M}} \right) \right]^{\frac{1}{2}} \left[\frac{I_{1M}}{I_{1d}} \right] \\ a_3 &= \left[\frac{1}{4\pi} \left(\frac{I_{3d}}{I_{3M}} \right) \right]^{\frac{1}{2}} \left[\frac{I_{2M}}{I_{2d}} \right] \end{aligned} \quad (4.2)$$

The products of the semi-axes $a_1 a_2$, $a_1 a_3$ and $a_2 a_3$, are obtained in appendix (D), and the relations (4.1), and (4.2), are determined solving the system of equations of the semi-axes products. In the current manuscript we are concerned with a specific issue, and we employ the semi-axes expressions given by equation (4.1), because we suppose that the spheroidal DM mass distribution analysed is well represented by such type of spheroid. The latter assumption is verified a posteriori by means of the DM fits and the determined DM halo resultant parameters. It is important to note that the results of this section as well as of the addendum (D), are general and independent of the particular matter studied in the present work, and therefore their applicability encompass a much more ample spectrum, than the simple example considered in the current analysis.

5 ROTATION FORMULA IN THE EQUATORIAL PLANE

In the present section we outline the region of the spheroidal mass distribution, where rotational motions should exist, and for that zone we determine an exact rotation formula, derived from the solution of the Poisson equation, obtained in section (3). The latter solution have to be specialised to a spheroidal system of orthogonal curvilinear coordinates, employing the diagonal solution of section (2.1), that transforms a non orthogonal system of curvilinear coordinates to orthogonal form. The triaxial spheroidal system of curvilinear coordinates we have selected is not orthogonal in its original configuration, and therefore it is necessary to apply the diagonalization relations determined in section (2.1), to

achieve its orthogonality. The diagonalization process employs the non diagonal expressions of the metric tensor matrix elements obtained in appendix (C), because the diagonalization formulas of section (2.1) are expressed as functions of the non diagonal metric tensor matrix entries. The relations of addendum (C), before to be inserted into the diagonalization expressions of section (2.1), have to be evaluated for certain azimuthal and zenithal angles, depending on the regions where the rotational motion could exist, and the precise details of that procedure together with the resultant relations are given in the subsequent part of this section.

In the equatorial plane (EP), the components of the angular momentum of a triaxial spheroid of non uniform density with respect to the x_1 and x_2 axes vanish, whereas the angular momentum component along the x_3 axis is different from zero, and therefore the rotation is parallel to the EP. In the meridional plane as well as in the corresponding perpendicular plane, the main rotation pattern is about the x_2 and x_1 axes, respectively, and as a consequence the rotation is perpendicular to both planes. We particularise the velocity relations in the EP, because the RC is usually build from radial velocities on the sky, subtracted of the systemic, and de-projected to rotation and other possible components in the EP. We are aware that in the EP, the rotation coexists together with other types of motions, nevertheless the EP kinematics resembles much more than other planes the velocity field kinematics of an observed galaxy, for what noticed above about the angular momentum components, and consequently the velocity formula have to be computed in the EP. The latter evidence is also confirmed by theoretical studies of the evolution of stellar orbits into a non spherical gravitational potential well (Touma & Tremaine 1997). The starting point, for the computation of the velocity formula, is represented by the relation (3.1), the non orthogonal entries of the metric tensor matrix specialised for the azimuthal and zenithal angles of the EP, the elements of the orthogonal metric tensor matrix, calculated through the expressions (2.1), (2.2), and (2.3), as functions of the non orthogonal metric tensor matrix elements, and the DM haloes density profiles to be integrated to obtain the velocity relations according to the prescription of equation (3.1). The resultant equation that describes the rotational motion in the EP is reported below:

$$\frac{\partial \phi_1(v_1, 0, \frac{\pi}{2})}{\partial v_1} = \sqrt{\frac{V_{11}}{V_{22}V_{33}}} [GM_{DM}(v_1) + C_1] \quad (5.1)$$

where the quantity $M_{DM}(v_1)$ is the DM mass density, that can be determined for each DM halo through the integration of the DM haloes density profiles. The RC of each DM halo, is measured on segments that are parallel to the semi-minor axis, and the latter fact explains the selection of the azimuthal angle $v_2 = 0$. The choice of the EP sets the zenithal angle $v_3 = \frac{\pi}{2}$. The square root containing the term of the diagonal metric tensor matrix is computable from the relations of section (2.1), and the resultant DM models RCs,

considering only the Poisson part of the solution, i.e. $C_1 = 0$, are given by the following relation:

$$v_1 \frac{\partial \phi_1(v_1, 0, \frac{\pi}{2})}{\partial v_1} = \frac{GM_{DM}(v_1)}{v_1} \frac{a_1}{a_2 a_3} \quad (5.2)$$

The triaxial spheroid semi-axes a_1, a_2, a_3 that enter into equation (5.2), are parametrized according to the recipe disclosed in section (4), specifically are expressed as quotients of the initial fitting parameters, such as the initial DM halo masses, scale radii, and the derived initial volume densities. It is important to clarify that the DM halo masses and scale radii represent the solely free parameters of the fitting process of the DM RCs of UGC 8490 and UGC 9753, and the triaxial spheroid semi-axes are connected to the variations of those two free parameters through the relations given in section (4), and determined in appendix (D). The optimal fitting DM halo masses and scale radii, obtained as a result of the DM RCs fitting process of UGC 8490 and UGC 9753, determine the values of the DM haloes semi-axes, to unveil the actual spatial configuration of the DM mass density of both galaxies. We employ equation (5.2), to perform the fit of the DM RCs of UGC 8490 and UGC 9753. The details of the fitting procedure, and the resultant total and DM masses of UGC 8490 and UGC 9753, as well as, the overall DM mass distribution, for each DM model considered, are given in the next section.

6 APPLICATION TO THE DM RCs FIT OF UGC 8490 AND UGC 9753

The resultant DM halo mass and scale radius of every DM velocity profile considered in this study, are of great importance to discriminate among the sort of inner mass aggregation, and the spherical and oblate/prolate triaxial spheroidal solutions. In the subsequent parts of the present section we delineate primarily the Fourier analysis of the velocity fields of both galaxies to validate the hypothesis that the gaseous components are moving on nearly circular orbits, the fitting methodology, the DM models utilised, the necessary restrictions on the triaxial spheroid semi-axes, and the principal results attained. In the following we provide in tabular form the triaxial spheroidal DM masses and scale radii, whereas the best DM models fits are reported in graphical form. In this section we take advantage of the DM RCs of UGC 8490 and UGC 9753, determined by RP18, all the details about the derivation of both DM RCs, together with other important related things can be found in RP18. The current research could be considered as an improvement and extension of some fundamental aspects of the analysis of RP18.

6.1 Fourier analysis of the velocity fields of UGC 8490 and UGC 9753

We apply the methodology of Schoenmakers et al. (1997) (Sh97) to accomplish a Fourier harmonic analysis of the HI radial velocity fields of UGC 8490 and UGC 9753. The Sh97 technique is available through the *reswri* package, that forms part of the Groningen Image Processing System (GIPSY) (van der Hulst et al. 1992; Vogelaar & Terlouw 2001). The

strategy of Sh97, measures the deformation induced by a triaxial non spherical perturbation to the original axisymmetric gravitational potential, representing the non axisymmetric perturbation as a sum of Fourier harmonic components. The harmonic fit to the HI velocity fields of UGC 8490 and UGC 9753, should detect possible deviation from axisymmetry in the gravitational potential of both galaxies, to determine the amplitude of the radial motions associated with the kinematics of the gaseous components, and the corresponding elongation of the resultant gravitational potentials. Adopting the notation of Sh97, we denote with ϵ_{pot} the elongation of the global gravitational potential, and with φ_2 , an angular quantity, that is related to the azimuthal angle and the observer angle of sight.

The accomplished harmonic analysis of the HI velocity fields of UGC 8490 and UGC9753 ascertains that their average gravitational potential elongation is 0.034 ± 0.013 , and 0.025 ± 0.014 , respectively, and therefore the approximation of nearly circular orbits for the HI gas components of both galaxies is adequate enough to describe the global motion of the neutral hydrogen of UGC 8490 and UGC 9753. The corresponding radial plots of the gravitational potentials elongations of both galaxies are displayed in figure (1).

6.2 Fitting strategy and semi-axes settings

The fits to the HI and H α DM RCs of UGC 8490 and UGC 9753 were performed through the *minuit* fitting routine, that is part of the ROOT package (Brun & Rademakers 1997), a versatile data analysis tool created at CERN. We made use of five DM models, expressly, the NFW, BKT, DCN, EIN, and STD DM haloes.

In the present work we prefer to fit separately the H α and HI RCs, because as detailed in section (7.2), the HI disc of both galaxies displays a very perturbed dynamics, in contrast, the H α disc of UGC 8490 and UGC 9753 exhibits a much more quiet dynamical behaviour, and therefore we argue that the two gaseous tracers should not necessarily describe exactly the same gravitational potential, and as a consequence we perform the fits of the H α and HI DM RCs.

The adopted fitting methodology can vary an indefinite number of parameters, nonetheless the DM models of NFW, BKT and DCN are characterised by two fundamental quantities, the DM halo mass and scale radius, whereas the DM halos of EIN and STD present an additional parameter that controls the spatial mass density arrangement of the DM halo, and as a consequence, for the EIN and STD DM halos there are three free parameters. The resultant EIN shape parameter converged to the values of 2.3 and 3.9, 5.0 and 1.4, for the triaxial spheroidal fits to the H α and HI DM RCs of UGC 8490 and UGC 9753, separately, whereas the final STD λ parameter converged to the values of 3.7 and 4.4, 5.7 and 3.5, for the triaxial spheroidal fits to the H α and HI DM RCs of UGC 8490 and UGC 9753, respectively. We have to clarify that the values of the EIN form parameters, determined through our fitting analysis, are in total agreement with the outcomes of the Cold DM N-body numerical simulations of Navarro et al. (2004), and Dutton & Maciò (2014) (DM14), given that, the EIN density profile, that those authors employ has the reciprocal shape index with respect to our profile, as also observed by Chemin et al. (2011) (CH11). The STD λ index is also concordant with

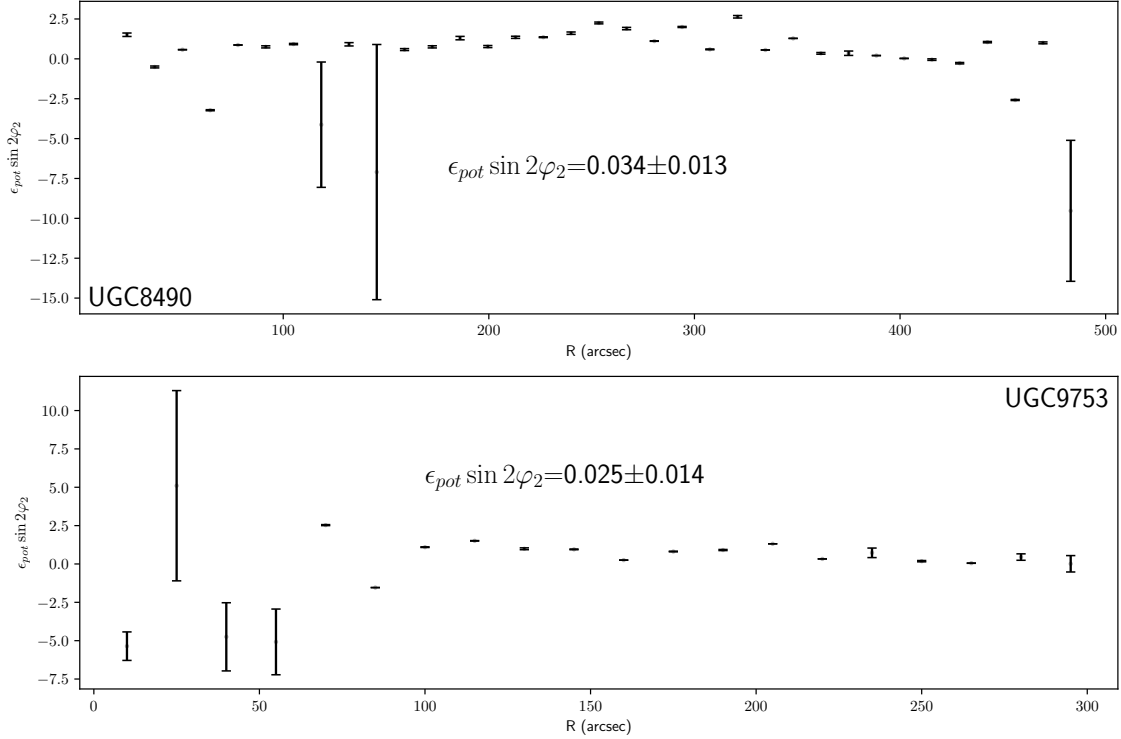


Figure 1. Gravitational potential elongation as a function of radius for UGC 8490 and UGC 9753. The exact values of the elongation together with the respective errors are showed within the figures. The elongation values are less than 0.1, and therefore we conclude that the gravitational potential is globally axisymmetric and that the gas orbits are well approximated by circles.

the prescription of STD, given that in the velocity formula derived in Repetto et al. (2015), the STD index appear as the reciprocal of the STD index λ . We found different values of the indexes parameters of EIN and STD, for the H α and HI RCs of UGC 8490 and UGC 9753, and a possible interpretation could be that the two distinct tracers denote different parts of the same gravitational potential, as partially confirmed by the fact that the resulting H α and HI DM masses and scale radii delineate a dissimilar DM mass density distribution among the H α and HI gaseous tracers.

The range of variation of the DM haloes mass and radius is $[10^8, 10^{13}] M_\odot$ and $[0.1, 500.0]$ kpc, respectively.

The fitting procedure have two important indicators to decide if a given solution can be considered satisfactory, the reduced χ_r^2 , that are χ^2 normalised for the number of degrees of freedom, and the estimated distance to the minimum (EDM). In the current work we reformulate the χ^2 definition, adopting the square root of the observed DM RCs data as the divisor of the differences between the DM models and the DM RCs data, and the resultant χ_r^2 values seem more concordant with the quality of the presented DM RCs fits. The EDM values are determined on the base of a Monte Carlo search, associated to a Metropolis minimization algorithm, that repeatedly measures the minimum distance

among all the solutions found through the fitting process, to ascertain the best possible minimization result.

The definition of the oblate and prolate spheroids employed in the present work, relies on the values of the semi-axes a_3 , and it is dependent on the initial values of the DM fitting masses, scale radii, and corresponding spatial densities, as well as, their evolution during the fitting process, as we explain in more detail below. The initial values of the DM masses and scale radii of every DM halo, produce, at first, a triaxial DM configuration, that evolves according to their variation. The details about the triaxial spheroid semi-axes prescriptions, as a parametrization of the DM models masses and scale radii, are outlined in the following. As already mentioned in section (4), the semi-axes of the supposed triaxial spheroid are parametrized by the DM haloes masses, scale radii, and corresponding volume densities, that originate from the fitting process to the DM RCs of UGC 8490 and UGC 9753. The integral quotients that enter in the definition of the triaxial spheroid semi-axes, delineated by equations (4.1), and (4.2), can be expressed as adimensional ratios of the resulting fitting parameters, according to the following prescription:

$$\frac{I_{xM}}{I_{xd}} = \alpha_x \frac{M}{\rho v^3} \quad \frac{I_{xd}}{I_{xM}} = \frac{1}{\alpha_x} \frac{\rho v^3}{M} \quad (6.1)$$

where the constant α varies depending on the DM models and other factors, explained below. The differences, in the values of the constant α for distinct DM models, are due to the dissimilar constants that define the five DM haloes density profiles analysed in this work. The subscript x indicates the diverse magnitudes of the integral ratios depending on the three distinct mass density symmetries considered within the triaxial spheroid, and defined through the three principal axes of symmetry, respectively. The relations (6.1) represent a compact form to express the integrals ratios, in the actual relations that we employed in the fit of the DM RCs of UGC 8490 and UGC 9753, the constants α , are known real numbers for every DM halo studied, and their exact numerical values also comprehend the differences of amplitudes originated by the distinct volume density symmetries selected to determine the semi-axes products (e.g. appendix (D)). The resultant semi-axes values of each DM fit, are reported in table (1), together with the corresponding DM masses, scale radii, and derived volume densities. We employ as fitting formula the relation (5.2), specialised to the particular mass distribution of each DM halo, and with semi-axes parametrized according to the prescriptions delineated above and in section (4). As in RP18 we adopt the approximation of DM14 for the concentration parameter of the NFW DM halo, the DCN circular velocity is that of Kravtsov et al. (1998) (KT98), and we employed the approximations of Ciotti & Bertin (1999) and of MacArthur et al. (2003) for the quantity d_α of the EIN DM model, in their respective regimes of validity.

6.3 Best fitting models and resultant DM masses, scale radii and semi-axes

The description of the most important results include some necessary specifications about the best DM models, based on the χ_r^2 , EDM values, visual quality of the fits and the number of points of the χ^2 contours plots, since all those quantities together, establish the reliability of a given solution, for every DM model studied in this manuscript. In addition, we present graphically the best fitting DM haloes, and we enumerate in four tables the totality of the fitting results.

In the verbal account of the principal results, we emphasize two fundamental distinctive attribute that every best fitting solutions should have, mainly depending on the intrinsic properties of the selected DM halo profiles, namely, the cuspy or core behaviour. The latter difference is of great relevance to determine, as accurate as possible, the inner DM density profile, and as a consequence to know whether the observed DM mass in the interiors of the studied galaxies has a finite or infinite amount. The further distinction among the spherical, oblate or prolate spheroidal character of the best solutions is also of great importance to determine the overall most probable DM mass distribution for UGC 8490 and UGC 9753.

The total baryonic masses of UGC 8490 and UGC 9753 are estimated according to the methodology explained in RP18 and their respective values and deviations are

$(2.4 \pm 0.3) \times 10^9 M_\odot$ and $(2.0 \pm 0.3) \times 10^{10} M_\odot$, separately. The total stellar and gas masses of UGC 8490 and UGC 9753 are $\approx 2.8 \times 10^8 M_\odot$ and $2.2 \times 10^9 M_\odot$, and $\approx 3.6 \times 10^9 M_\odot$ and $1.6 \times 10^{10} M_\odot$, respectively. The total mass of both galaxies is obtained by the sum of the total baryonic mass and the determined DM masses for each DM models adjusted. We refer, the interested reader, to sec. 4 of RP18 for the methodology employed to obtain the stellar RCs, the HI+He+metals RCs, the DM RCs of both galaxies, that are displayed in Fig. 2, and Fig. 4, and all the relevant details concerning for instance the M/L ratios. As already explained in RP18, we obtain the stellar RCs of UGC 8490 and UGC 9753, from stellar population synthesis studies, and we take into account the corresponding uncertainties once we build the 2D stellar maps, and then the stellar RCs. The HI+He+metals RCs are determined through the 2D HI total density maps, together with the relative errors, connected to distances, inclinations and position angles, as for the stellar RCs. The DM RCs of both galaxies are obtained subtracting the stellar RCs from the observed H α RCs, and the stellar and HI RCs from the observed HI RCs. In our methodology, we do not consider the stellar and gaseous parts of a galaxy as parametric curves, instead, we prefer to obtain the baryonic portions of our galaxies from photometric and spectroscopic measurements of the respective stellar and gaseous components.

The fitting process of the H α and HI DM RCs of UGC 8490 and UGC 9753, determines that the overall DM distribution of both galaxies is adequately represented by oblate spheroids, whose semi-axes have different values depending on the galaxy and the DM model considered. The corresponding semi-axes, together with the respective uncertainties are tabulated together with all the other results in Tables 1, 2, 3, and 4.

The principal results for the triaxial spheroidal DM fits to the H α and HI DM RCs of both galaxies are listed in Tables 1, 2, 3 and 4, separately, and as it is evident from the tabulated χ_r^2 , EDM, the DM RCs fits, and the χ^2 contours, displayed in Figs. 2, 4, 3 and 5, respectively, the best fitting solutions are those of cored BKT and cuspy DCN, with an inner slope of 1.3, for the H α DM RCs of UGC 8490 and UGC 9753, respectively. The cuspy DCN of inner slope 1.2, and the cuspy NFW represent the best fitting solutions for the HI DM RCs of UGC 8490 and UGC 9753. The inward DM distribution of both galaxies is characterised either by a cored DM density profile, or a cuspy one, and both solutions seem reasonable based on the corresponding DM masses and scale radii, reported in the respective tables.

In summary, the results of the current section establish a global oblate spheroidal DM configuration for UGC 8490 and UGC 9753, and a cored and cuspy inner DM distribution. The validation of the strategy employed to obtain the semi-axes values is performed in the next section through the application of a standard methodology that computes the resultant torques originated by the encounters among the hypothetical collisionless collective stellar and DM motions and the random displacements of the gaseous components.

Table 1. DM and total mass of UGC 8490: H α RC

DMHs ⁽¹⁾	M _T ⁽²⁾	M _{DM} ⁽³⁾	R _h ⁽⁴⁾	a ₁ ⁽⁵⁾	a ₂ ⁽⁶⁾	a ₃ ⁽⁷⁾	χ_r^2 ⁽⁸⁾	EDM ⁽⁹⁾
NFW	11.7 \pm 2.8	11.5 \pm 2.8	231.5 \pm 22.2	40.2 \pm 2.4	40.2 \pm 2.4	3.2 \pm 0.2	0.7	2.3 \times 10 ⁻⁸
BKT	0.2 \pm 0.03	0.04 \pm 0.003	1.6 \pm 0.06	23.0 \pm 0.6	23.0 \pm 0.6	1.8 \pm 0.05	0.96	5.0 \times 10 ⁻⁷
DCN	0.9 \pm 0.05	0.7 \pm 0.02	13.0 \pm 0.1	104.1 \pm 0.6	104.1 \pm 0.6	8.3 \pm 0.05	0.6	1.6 \times 10 ⁻¹⁰
EIN	0.3 \pm 0.04	0.05 \pm 0.007	9.0 \pm 0.6	14.0 \pm 0.6	14.0 \pm 0.6	1.1 \pm 0.05	0.8	2.2 \times 10 ⁻⁷
STD	0.8 \pm 0.1	0.6 \pm 0.07	8.6 \pm 0.5	16.0 \pm 0.6	16.0 \pm 0.6	1.3 \pm 0.05	0.74	1.2 \times 10 ⁻⁹

¹ DM haloes.² Total mass in units of 10¹⁰ (M_⊙).³ DM mass in units of 10¹⁰ (M_⊙).⁴ DM scale radius (kpc).⁵ DM halo major axis.⁶ DM halo axis orthogonal to the major axis on the EP.⁷ DM halo axis orthogonal to the EP.⁸ Reduced χ^2 .⁹ Estimated distance to the minimum.**Table 2.** DM and total mass of UGC 9753: H α RC

DMHs	M _T	M _{DM}	R _h	a ₁	a ₂	a ₃	χ_r^2	EDM
NFW	2.5 \pm 0.3	0.5 \pm 0.03	57.0 \pm 1.7	212.0 \pm 4.1	212.0 \pm 4.1	17.0 \pm 0.3	0.82	1.7 \times 10 ⁻⁹
BKT	2.1 \pm 0.3	0.06 \pm 0.004	1.2 \pm 0.03	34.0 \pm 0.6	34.0 \pm 0.6	2.7 \pm 0.05	6.6	2.0 \times 10 ⁻⁸
DCN	8.0 \pm 0.4	6.0 \pm 0.05	23.0 \pm 0.2	52.0 \pm 0.6	52.0 \pm 0.6	4.1 \pm 0.05	1.0	9.9 \times 10 ⁻⁹
EIN	2.1 \pm 0.3	0.08 \pm 0.008	12.0 \pm 0.5	21.0 \pm 0.6	21.0 \pm 0.6	1.6 \pm 0.05	1.6	5.1 \times 10 ⁻⁷
STD	2.6 \pm 0.3	0.6 \pm 0.04	7.8 \pm 0.2	23.3 \pm 0.4	23.3 \pm 0.4	1.9 \pm 0.04	6.6	2.5 \times 10 ⁻⁷

Table 3. DM and total mass of UGC 8490: HI RC

DMHs	M _T	M _{DM}	R _h	a ₁	a ₂	a ₃	χ_r^2	EDM
NFW	1.0 \pm 0.08	0.8 \pm 0.05	82.5 \pm 2.6	139.0 \pm 3.0	139.0 \pm 3.0	11.0 \pm 0.2	1.0	3.1 \times 10 ⁻⁷
BKT	0.28 \pm 0.03	0.04 \pm 0.003	2.1 \pm 0.07	25.7 \pm 0.6	25.7 \pm 0.6	2.0 \pm 0.05	0.98	1.5 \times 10 ⁻⁷
DCN	0.6 \pm 0.1	0.4 \pm 0.07	8.9 \pm 0.2	29.6 \pm 0.6	29.6 \pm 0.6	2.4 \pm 0.05	1.0	1.4 \times 10 ⁻⁶
EIN	0.3 \pm 0.05	0.1 \pm 0.02	34.0 \pm 1.9	11.8 \pm 0.4	11.8 \pm 0.4	0.94 \pm 0.04	0.75	1.1 \times 10 ⁻⁷
STD	1.2 \pm 0.09	1.0 \pm 0.06	23.5 \pm 0.7	29.9 \pm 0.6	29.9 \pm 0.6	2.4 \pm 0.05	0.8	5.0 \times 10 ⁻⁹

7 SEMI-AXES DETERMINATION THROUGH THE TORQUE METHOD

In the current section we determine the semi-axes values by means of a widely known alternative methodology, that computes the torques produced by the dynamical interactions between the gaseous and stellar phases, of UGC 8490 and UGC 9753, that move under the gravity of the corresponding DM haloes. The dynamical interplay among the globally ordered stellar motions and the haphazard gas movements, should delineate the approximate extension of the DM halo gravitational influence. The corresponding induced perturbation, exerted on the galactic baryonic constituents, should leave direct evidences of the spatial distribution of the DM halo mass density on the baryonic stellar gravitational potential (e.g. Bekki & Freeman 2002; McQuinn et al. 2015; Hu & Sijacki 2016).

The specific application of the torques procedure to UGC 8490 and UGC 9753, is accomplished according to the prescription of García-Burillo et al. (2005), in particular we compute the gravitational potential maps (GPM) of both galaxies from K band 2MASS (Skrutskie et al. 2006) images of UGC 8490 and UGC 9753, through the integral relation of Binney & Tremaine (2008, Chapter 2,

pag. 56, eq. 2.3), supposing a M/L of unity, after proper de-projection, sky subtraction and elimination of any irregularities through appropriate operations of masking and clipping. The photometric de-projection parameters obtained from the HYPERLEDA¹ astronomical database (Makarov et al. 2014), are position angles and inclinations of 5.5, 1.5° and 58.8, 72.7°, for UGC 8490 and UGC 9753, respectively. We performed the sky subtraction using the sextractor package (Bertin & Arnouts 1996). We perform a Fast Fourier Transform of the GPM of both galaxies, and we determine the corresponding amplitudes, phases, and the central frequencies, to build the Fourier series expansions (FSE) of the GPM of UGC 8490 and UGC 9753. Once we have determined the FSE of the GPM of both galaxies we proceed to obtain the gradients of the latter maps to ascertain the forces components along the abscissa and the ordinate directions. The torque map of UGC 8490 and UGC 9753 is determined by means of the standard relation, and from those maps we measure the semi-axes of the triaxial spheroidal perturbation. It is worth to notice that

¹ <http://leda.univ-lyon1.fr/>

Table 4. DM and total mass of UGC 9753: HI RC

DMHs	M_T	M_{DM}	R_h	a_1	a_2	a_3	χ_r^2	EDM
NFW	63.4 ± 0.8	61.4 ± 0.5	500.0 ± 4.2	192.0 ± 1.8	192.0 ± 1.8	15.0 ± 0.1	0.97	2.8×10^{-9}
BKT	2.5 ± 0.4	0.5 ± 0.1	10.6 ± 1.1	8.9 ± 0.6	8.9 ± 0.6	0.7 ± 0.05	0.72	8.2×10^{-9}
DCN	12.0 ± 0.9	9.9 ± 0.6	96.0 ± 2.4	35.1 ± 0.6	35.1 ± 0.6	2.8 ± 0.05	0.76	6.0×10^{-9}
EIN	3.2 ± 0.6	1.2 ± 0.3	39.0 ± 3.7	6.5 ± 0.4	6.5 ± 0.4	0.5 ± 0.03	0.74	1.3×10^{-8}
STD	6.6 ± 1.2	4.6 ± 0.9	39.0 ± 3.4	10.3 ± 0.6	10.3 ± 0.6	0.82 ± 0.05	0.96	2.8×10^{-10}

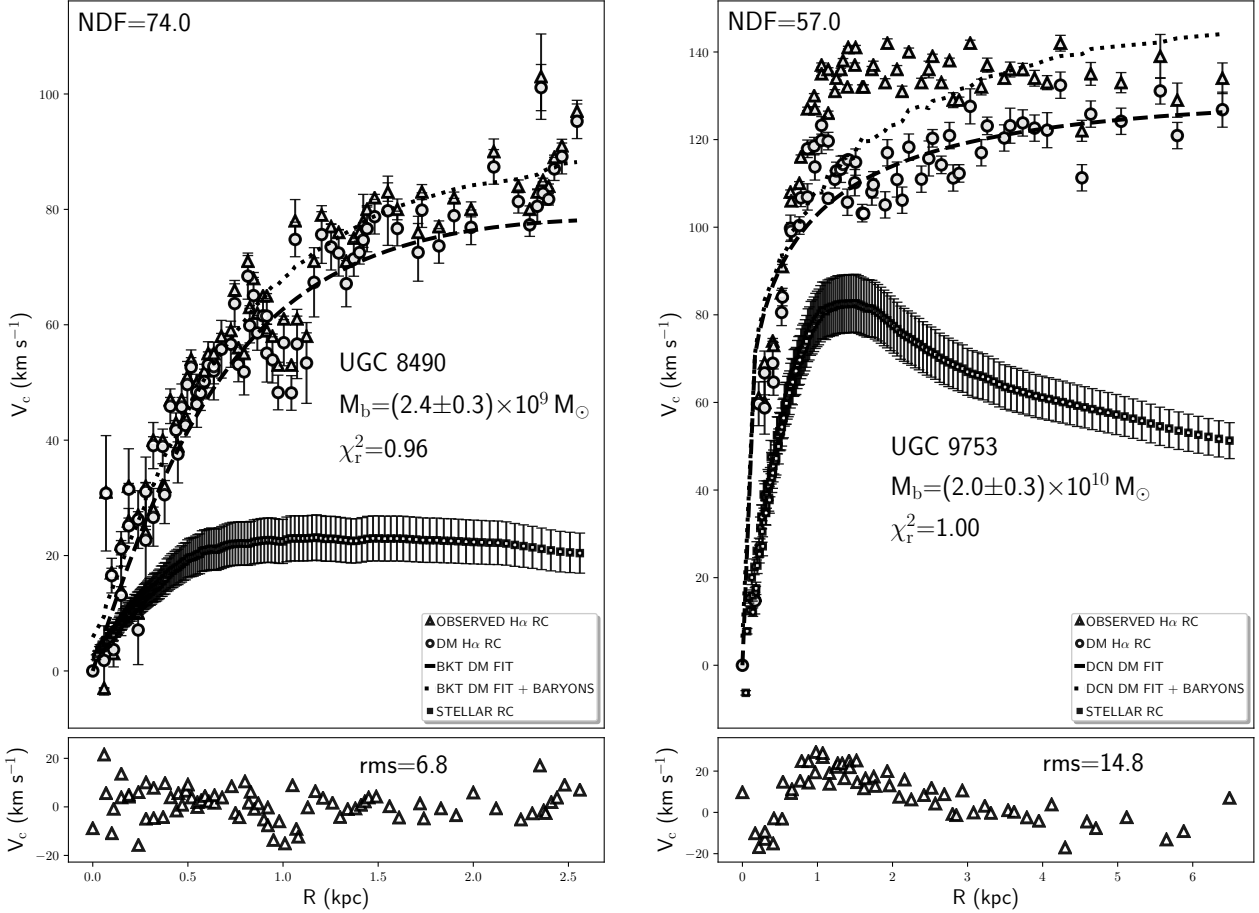


Figure 2. *Left:* BKT DM fit (dashed line) to the H α DM RC of UGC 8490. The observed H α RC is displayed together with the H α DM RC of the same galaxy. The dotted line denotes the BKT DM fit to the H α DM RC plus the stellar RC. The residuals in the lower panel represent the subtraction of the squared BKT DM fit to the H α DM RC plus the squared stellar RC, from the squared observed H α RC. *Right:* Identical information for the DCN DM fit to the H α DM RC of UGC 9753.

the torque component we have obtained is the one perpendicular to the galactic plane. We determine the semi-axes of the torque perturbation, in the EP of UGC 8490 and UGC 9753, from the torques maps of each galaxy, through the IRAF STSDAS Ellipse fitting procedure. The semi-axes perpendicular to the EP of both galaxies, are obtained fitting the vertical profiles of the torques maps of UGC 8490 and UGC 9753, that originate from the torque perturbation, and represent well discernible features in the torques maps. The corresponding values of the semi-axes of the torque perturbation of UGC 8490 and UGC 9753 together with their

respective uncertainties are $a_1=11.0 \pm 0.3$, $a_2=10.9 \pm 0.23$, and $a_3=3.5 \pm 0.12$, and, $a_1=28.2 \pm 0.8$, $a_2=27.9 \pm 0.7$, and $a_3=0.7 \pm 0.06$, for UGC 8490 and UGC 9753, respectively. The gravitational torques maps of UGC 8490 and UGC 9753 are displayed in figure (6) and (7), and the nearly circular area of those figures, highlighted by dashed circles, indicate the regions of the discs of both galaxies where the torque perturbation is stronger. The average of the semi-axes ratios derived from the fits to the H α and HI DM RCs of UGC 8490 and UGC 9753 are $\frac{a_2}{a_1}=1.0$, $\frac{a_3}{a_1}=0.08$, and $\frac{a_3}{a_2}=0.08$, correspondingly, the average of the semi-axes ra-

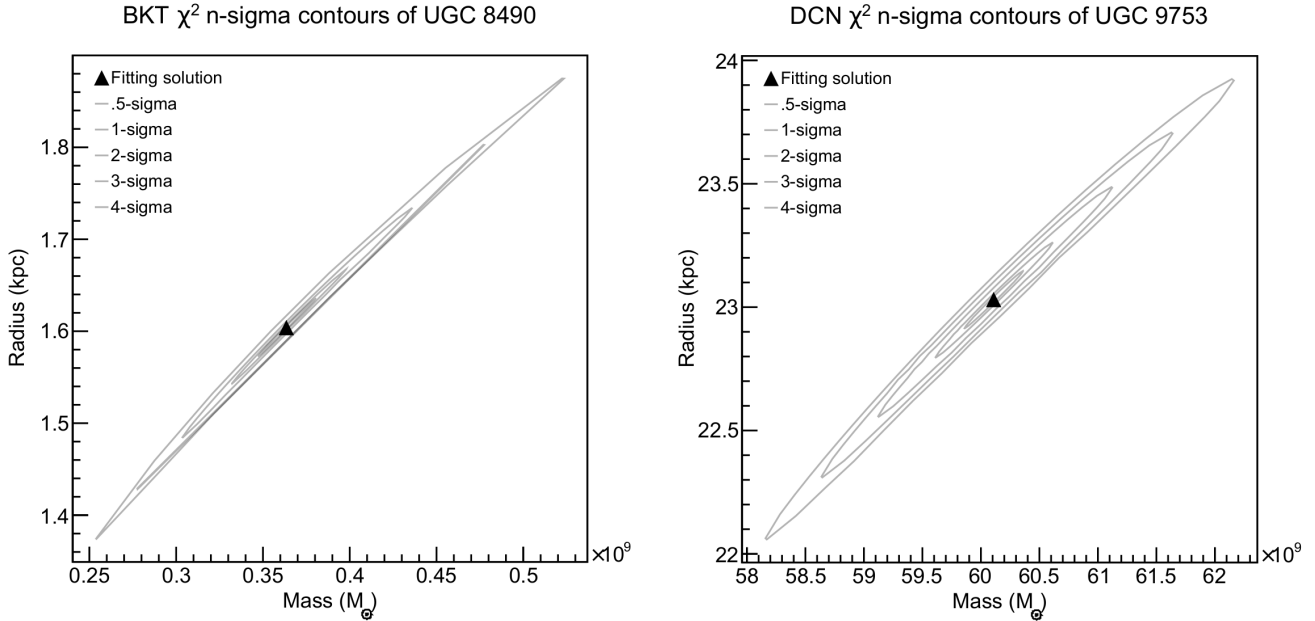


Figure 3. *Left:* BKT χ^2 n-sigma contours of the BKT DM fit to the H α DM RC of UGC 8490. The contours ellipses represent five χ^2 error contour levels. The solution is indicated by a black filled triangle and lies within the 0.5-sigma contour level, where the optimal solution is expected to stay. *Right:* Identical information for the DCN χ^2 n-sigma contours of the DCN DM fit to the H α DM RC of UGC 9753.

tios of the two galaxies, obtained from the torque method, are $\frac{a_2}{a_1}=1.0$, $\frac{a_3}{a_1}=0.17$, and $\frac{a_3}{a_2}=0.17$. The semi-axes values of the DM haloes of UGC 8490 and UGC 9753 describe an oblate DM mass configuration for the two galaxies analysed in this work, and the corresponding mean semi-axes ratios are approximately concordant with the average semi-axes ratios obtained through the fits to the DM RCs of UGC 8490 and UGC 9753, and as a consequence the results about the spatial configuration of the DM density of UGC 8490 and UGC 9753, obtained through the application of the torque method are in general consistent with the corresponding outcomes of the DM fits to the RCs of both galaxies.

The small discrepancy among the semi-axes values obtained through the DM fits and by means of the torque procedure, should not be a matter of great concern, given that, as explained in the subsequent part of the current section, the two methodologies employed, to obtain the semi-axes values, analyse very distinct phenomenologies to determine the semi-axes values, and consequently, the results are not expected to be exactly the same. It is evident that the determination of the DM halo semi-axes through the torque method and by means of the fits to the DM RCs of UGC 8490 and UGC 9753, is based on the analysis of very different phenomena and associated physical processes, given that the DM RC is a measure of the mass density and extent of a hypothetical virialised density aggregation, whereas the torque method is related to the interaction among different galactic components, and therefore describes phenomena that are far from any sort of balance among the gravitational forces that determine the dynamics of the distinct galactic constituents, and consequently the out-

comes of the two strategies should not necessarily produce similar results.

7.1 Synthetic data tests: self-generated data and TNG Illustris data

In the following, we present a short description of the artificial data trials we have performed to evaluate the accurateness of the strategy devised in this study, whereas, the complete description of those experiments is provided elsewhere.

Self-generated DM data: we build mock NFW DM RCs considering spherical, oblate and prolate mass density distributions, and we fit those artificial data employing the rotation formula defined by equation (5.2), to determine the robustness of the proposed methodology. We expect that whether the resultant DM masses and scale radii, retrieved by the fitting procedure, are equal to those settled to build the mock DM RCs data, then the final semi-axes values have to coincide with those adopted to generate the synthetic DM RCs. The fits to the NFW DM RCs produces some specific values of the DM halo masses, scale radii and the corresponding semi-axes, and, any time that the resultant DM masses and scale radii are closer or identical to those of the mock data, the correspondent semi-axes are very similar or equal to those of the synthetic DM RCs. As a further experiment we compute the semi-axes values employing the DM masses and scale radii, originated through the fitting process, that present greater dissimilarity with respect to those of the artificial DM RCs, originally created, and we obtain semi-axes values that coincide with the outcomes of the fitting procedure.

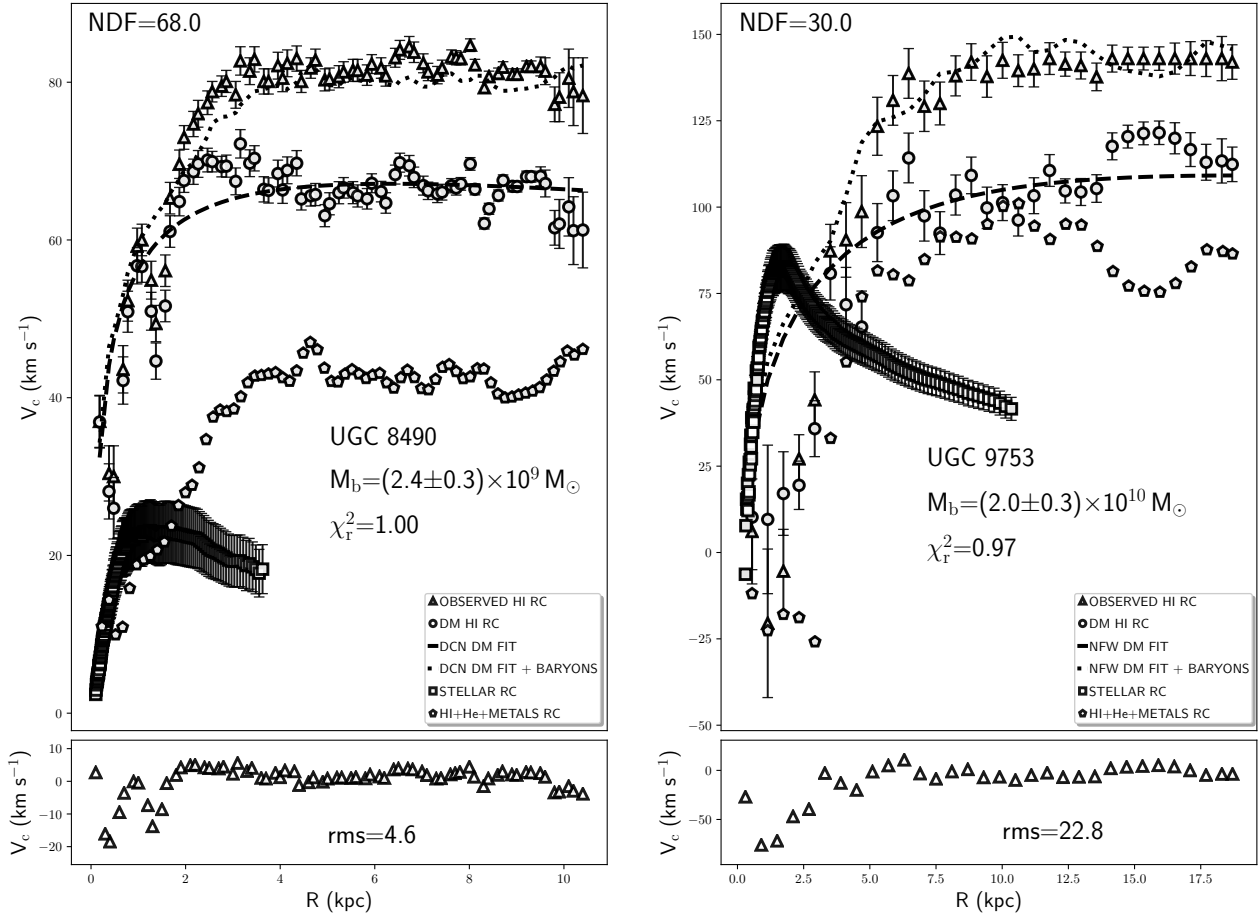


Figure 4. Identical information of Fig. 2 for the DCN and NFW DM fit to the HI DM RC of UGC 8490 and UGC 9753, respectively.

TNG Illustris low resolution DM data: we take advantage of the TNG-100-3 DM data (Nelson et al. 2019; Pillepich et al. 2018; Springel et al. 2018; Nelson et al. 2018; Naiman et al. 2018; Marinacci et al. 2018), to build and fit a spherical DM RC to determine the semi-axes values following the methodology proposed in section (4) and (5) of the present manuscript. The complete details about the analysis of the TNG Illustris DM data, the fitting procedure of the determined DM RC, and the principal results, are given in a separate document, as already stated above. The main outcome of the performed experiment with the TNG Illustris simulation DM data, indicates total concordance with the paramount findings of this study, and the test performed with self-generated DM data. The resulting parameters (in particular the EIN shape index) of the EIN fit to the TNG Illustris simulated DM RC, that we have extracted and examined in the current tryout, are consistent with the findings of CH11, specifically their section 6.1, and Tissera et al. (2010).

The general conclusion is that the semi-axes expressions determined in the present work, represent a very solid instrument to analyse the DM halo spatial structure, at least from the perspective of a DM RCs fitting analysis. The principal results of this section constitute additional evidences that support the methodology conceived in this study.

7.2 Comparison with other works

In this section we contrast the fitting results for UGC 8490 with the outcomes of other studies in the current literature, in particular, with the researches of Li et al. (2018) (L18), and Ren et al. (2019) (R19), and in general with other works that perform Cold DM, and Cold DM hydrodynamical simulations, to analyse the different properties of DM halos without and with baryons, especially, the DM halo spatial structure. The comparison for UGC 9753 is not possible, because, in the present literature does not exist any research work, that deals with the DM halo shape, or in general with the content of DM of that galaxy. As anticipated above, the contrast with UGC 8490 is feasible, and for that galaxy, we note a discrepancy among our M/L values, that vary in the range ~ 0.2 - 0.3 and those of L18 and R19, that range in the intervals ~ 0.75 - 0.97 , and ~ 0.96 - 1.4 , and, those differences could be determined, for instance, by the different ingredients employed by those authors to build their stellar population synthesis models, such as, for example the selected initial mass function, the Hubble constant, and possibly others. It is important to emphasize that our M/L are in perfect agreement with those of de Blok et al. (2008), however they are slightly at variance with respect to those of

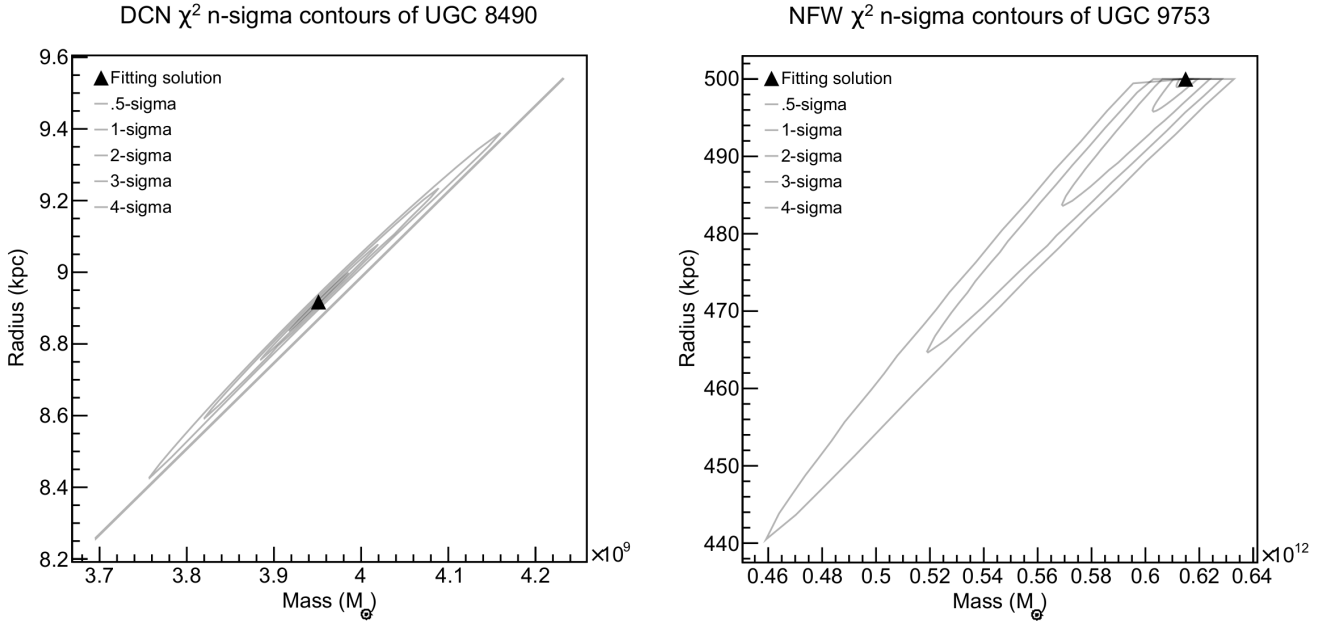


Figure 5. Identical information of Fig. 3 for the DCN and NFW DM fit to the HI DM RC of UGC 8490 and UGC 9753, respectively.

Oh et al. (2008), likely due to a different choice of the initial mass function, as explained in RP18. The DM masses and scale radii are not listed in the work of L18, therefore a direct comparison with those authors is not feasible, whereas our DM masses and scale radii are distinct from those of R19 (see their table S2), that employs a Self Interactive DM model coupled in the outer galactic parts with a NFW density profile, therefore we argue that the dissimilar modelling conditions, together with the diverse M/L ratio could determine the differences on the DM masses and scale radii. The comparison of our DM masses, scale radii, M/L ratios with those resulting from the work of Li et al. (2020) (L20), indicates higher baryonic disc M/L ratios with respect to our (contrast the M/L interval of ~ 0.5 -1.24 with the values ~ 0.2 -0.3 of RP18), and consequently the DM masses and scale radii of L20 vary from 2.5×10^{10} to $1.6 \times 10^{11} M_{\odot}$, and from 0.5 to 11.1 kpc, separately, and are definitively different with respect to the values reported in table 1, 2, 3 and 4, for the DM models of NFW, BKT, DCN and EIN, adopted by us and L20. The DM masses of L20 are higher than our values, and the latter fact seems consistent with the corresponding M/L ratios disparity between the L20 results and our findings.

The comparison with Cold DM and Cold DM hydrodynamic simulations produces a qualitative agreement with our results, given that those simulations predict nearly spherical or oblate DM halos, that predict triaxial DM halos at the present epoch (see for instance, Bryan et al. 2013; Brainerd & Yamamoto 2019; Chua et al. 2019; Artale et al. 2019; Drakos et al. 2019). The value of the ratio among the major and minor axis, determined through our analysis, seems to small when compared with the quoted studies that determine, a range of variation, of that quantity, about ~ 0.5 -0.7. The latter difference could be explained by the

kinematic and dynamic peculiarities of the baryonic discs of UGC 8490 and UGC 9753. Swaters et al. (2002) determines, from the HI global profile, that UGC 8490 is strong lopsided, furthermore, Sicotte & Carignan (1997), found a strong kinematic warp in the disc of UGC 8490, from HI observations. According to Karachentsev et al. (2003), UGC 8490 is part of the Canes Venatici I cloud, and as a consequence, could be affected by environmental phenomena that are typical of galaxy groups, such as, for instance, possible gravitational encounters with other group members. UGC 9753 is an active galaxy, in particular is an intermediate type between a Seyfert 2 and a LINER according to Ho et al. (1997), and is classified as a barred galaxy of moderate bar strength (bar index 0.5) by Buta et al. (2015). Di Teodoro & Fraternali (2014) found a very low rate ($\sim 0.01 M_{\odot} \text{ yr}^{-1}$) of HI accretion in the disc of UGC 9753, furthermore, Sengupta & Balasubramanyam (2006) reported that UGC 9753 belongs to a sparse group of galaxies, and determined that UGC 9753 possesses a dearth of HI of 0.12. The latter study reveals that the HI scarcity detected in UGC 9753, could be caused by tidal ram-pressure stripping, together with HI evaporation produced by kinetically transmitted heat. From the above quoted literature, it is evident that UGC 8490 and UGC 9753, present a very perturbed kinematic and dynamic scenario either within their galactic discs, or, in the surrounding environment, and, all the evidences seem to support the latter view, and, as a consequence, the small axial ratios among their minor and major axes, of the order of ~ 0.1 , could be connected to those disturbances, given that, according to the study of Putko et al. (2019), the actual shape of galaxies that have lopsidedness, gas accretion, and other kinematic and dynamic peculiarities, show the corresponding axial ratios of ≈ 0.15 , and even though, the latter result is related to the shape of the whole galaxy, it is well-

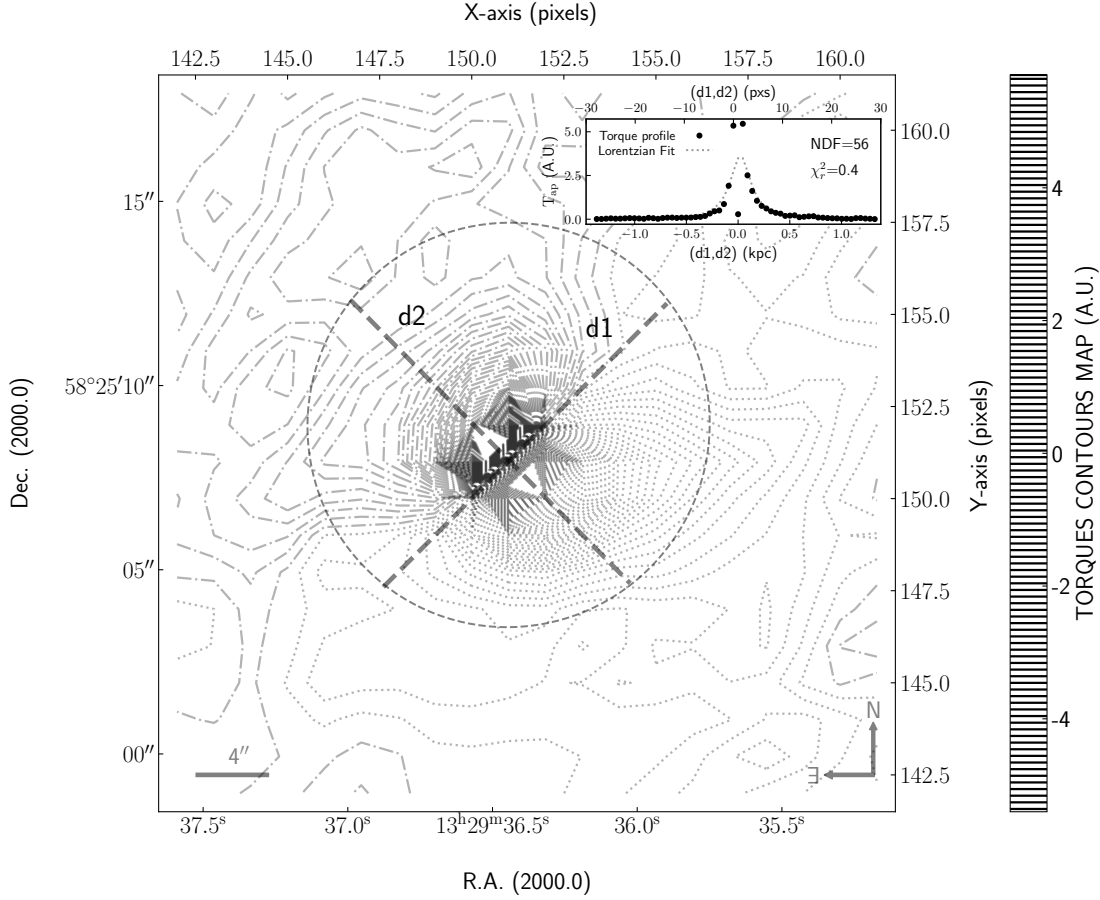


Figure 6. Torques map contours of UGC 8490, the contours levels range from -5.4 to 5.7 with a constant step of 0.1. The dashed region encloses the area of maximum perturbation induced by the torques computed at each pixel. The dotted contour lines indicates the zones where the gravitational torques field is negative, whereas the dash-dotted contour lines denotes the areas where the gravitational torques field is positive. The inserted panel shows the Lorentzian fit to the profile that represents the average of the two profiles extracted from the Torques map along the directions d1 and d2. The value of the Lorentzian peak corresponds to the length of the semi-axis of the triaxial spheroid perpendicular to the EP.

known, from numerical simulations, that the baryonic and DM components, can show similar spatial elongations (e.g. Velliscig et al. 2015). We conclude that our semi-axes ratios seem to be concordant with some author, and are congruent, with some observed properties of the baryonic discs of UGC 8490 and UGC 9753.

8 CONSIDERATIONS ABOUT SOME OF THE PRINCIPAL FINDINGS

In this section we discuss the principal results obtained in this work, particularly, the expansion of the most important parts of the methodology of RP18, that constitutes a fundamental piece of information for the specialisation of the determined gravitational potential relation to specific mass configurations, and the other important findings about the total and DM mass distribution of UGC 8490 and UGC 9753, that constitute an application of the procedu-

ral extension of RP18, accomplished in the first part of this study.

The general solution of the Poisson equation obtained in section (3), supposes that the adopted curvilinear coordinates system is orthogonal (i.e. that the associated metric tensor matrix is diagonal), or equivalently, that can be transformed into orthogonal form, through the diagonalization of the corresponding non diagonal metric tensor matrix. The advantage of this type of solution is that can be utilised to analyse the dynamics of several different 3D mass density distributions with given volume densities, and for the latter reason represents a very valuable tool to ascertain which kind of motions are feasible, within those mass density systems, based on the knowledge of the complete force fields of those density aggregations, and consequently of every dynamical and kinematical effects originated. The proposed solution of the Poisson equation determined in this article is also adequate to address dynamic and kinematic problems

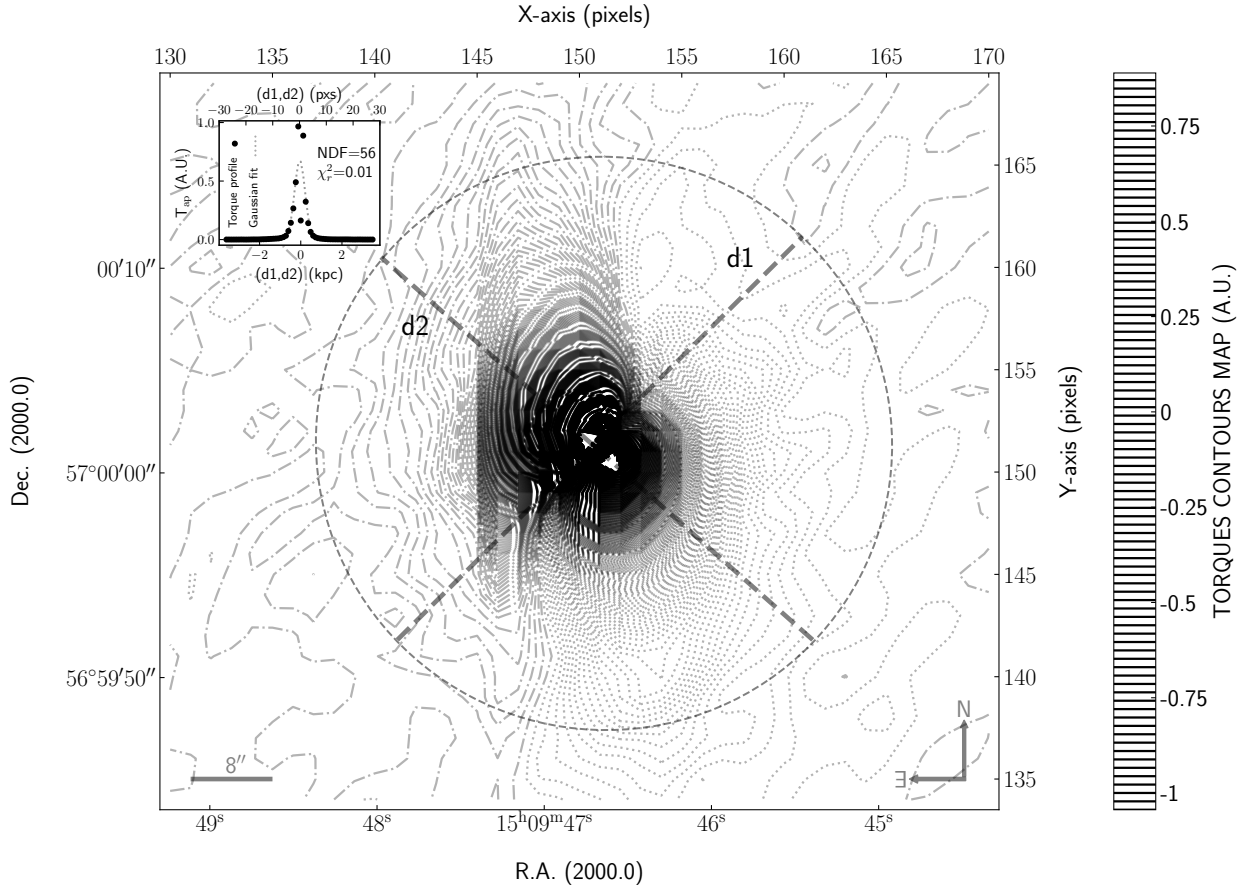


Figure 7. Identical information of Fig. 6 referred to the torques map of UGC 9753. The contours levels range from -1.04 to 0.9 with a constant step of 0.001. The contours levels interval indicated by the colorbar has a step of 0.022, that approximately corresponds to the differences among the contours levels steps of the contours map and the corresponding colorbar is necessary, on the one hand, to depict the entire area of the torque perturbation, and, on the other hand, to obtain a meaningful colorbar.

in 2D or 1D, as the application illustrated in the current work, clearly demonstrate.

It is important to clarify that we fit individually the $H\alpha$ and the HI DM RCs, of UGC 8490 and UGC 9753, because we want to analyse the DM haloes masses and scale radii, of both galaxies, in a separate manner, for the inner and outer regions of the disc of the analysed galaxies, to understand the principal differences between the interior and exterior DM mass density configuration of UGC 8490 and UGC 9753. The latter arrangement does not represent the standard practise (e.g. [Swaters et al. 2003](#)), nonetheless, according to us, it should be a more adequate way to study the actual clumpy structure of the conjectured DM haloes, and to analyse the interaction of the DM halo with distinct parts of the baryonic gravitational potential. We fit the same DM density profiles for the $H\alpha$ and HI DM RCs, and the DM masses and scale radii that result from the fits to the $H\alpha$ and HI DM RCs of UGC 8490 and UGC 9753 are indeed different, probably due to the fact that we measure diverse portions of the DM halo of each galaxy, that interact with those parts of the baryonic gravitational potential connected either to

the ionised or neutral hydrogen. The latter considerations are supported by several theoretical works that analyse the dynamical and kinematical properties of the DM haloes substructures, some of the most prominent research studies on that specific subject are, for instance, [Springel et al. \(2008\)](#); [Giocoli et al. \(2010\)](#); [Lange et al. \(2018\)](#), among many others.

Although in this work we cannot address the cuspy/core problem, for the reasons clearly stated in the introduction, it is worth to comment something about the DM RCs fitting outcomes. The results of the fits to the DM RCs of UGC 8490 and UGC 9753 establish that both core or cuspy inner slopes are acceptable to explain the inward DM distributions of UGC 8490 and UGC9753, the latter outcome is concordant with some recent works and the general view on the cuspy/core issue that has been developing during many years of research on the subject ([Oman et al. 2015](#); [Relatores et al. 2019](#); [Santos-Santos et al. 2019](#)). The current knowledge about the cuspy/core issue seems to indicate that the presence of a cored or cuspy DM density profile is dependent on the dynamical evolutionary state of the baryonic com-

ponent, along the galaxy formation history, in particular a crucial parameter is the gas density and its relation to the star formation process. The emergent picture suggests that, during the evolution of a galaxy, the core or cuspy behaviour is a transient feature related to the gas hydrodynamics and its connection to the evolutionary path of the stellar component (Benítez-Llambay et al. 2019; van Dokkum et al. 2019; Yeh & Jiang 2018).

The determination of the semi-axes of the supposed DM triaxial spheroid is performed by means of a novel procedure, delineated in section (4) and appendix (D), that parametrizes the three semi-axes as quotients of the DM haloes masses and scale radii, and the corresponding volume densities. The fitting procedure to the DM RCs of UGC 8490 and UGC 9753, varies at each fitting iteration the DM masses and scale radii and consequently generates new values of the three semi-axes, the resultant DM masses and scale radii determine the semi-axes that define the DM mass density spatial configuration of UGC 8490 and UGC 9753. The results obtained in section (6.3) favoured a flattened DM distributions for the two galaxies analysed in this work, and the successive comparison with the well known strategy of the gravitational torques, to obtain the global gravitational perturbation induced by the DM haloes on the baryonic components, confirms the findings of the fits to the DM RCs of UGC 8490 and UGC 9753. The methodology devised to obtain the DM haloes semi-axes as parametric ratios of the DM masses, scale radii and the corresponding volume densities, is substantially different from the analysis of the DM halo triaxiality based on the detection and measurement of the indirect gravitational effects produced by the DM component on the gaseous and stellar constituents of the galaxies under study, and in the subsequent part of this discussion we succinctly illustrate the principal differences, among the two strategies, and, at the same time, we highlight the advantages and the drawbacks of both approaches. The recipe ascertained in the current research, to determine the semi-axes of the hypothetical DM triaxial spheroid, estimates the total DM mass with respect to every axis of symmetry, taking advantage of the invariance of the total DM mass, for any single galaxy examined. The latter procedure does not assume total energy or angular momentum conservation, and does not suppose any particular kinematic degree of freedom, such as for instance rotation, vibration or others, furthermore, all the quantities involved are weighted for the spatial density, that defines the actual DM distribution, that could be completely asymmetric, regardless of the seeming symmetry that is inherent in the semi-axes computation. For all the reasons enumerated, the methodology devised in this work to obtain the semi-axes values of the spheroidal DM distribution of UGC 8490 and UGC 9753, seems adequate to be applied to issues connected with the DM in galaxies.

The comparison with the strategy of the gravitational torques seems satisfactory, nonetheless the exact values of the semi-axes obtained with the methodology devised in the current work do not coincide with those determined through the gravitational torques approach, and one of the possible reasons is that as partially explained at the end of section (7), they measure the same quantities, through the analysis of very different phenomenological and physical conditions, and therefore we expect only a qualitative concordance of the results. The two procedures determine that UGC 8490

and UGC 9753 present flattened DM distributions, nonetheless the strategy based on the fits of the DM RCs of the two galaxies, produces different semi-axes values for each DM density profile employed, whereas the gravitational torques method gives singular distinct values for each galaxy. The latter difference is an intrinsic feature of each one of the two approaches, due to the fact that the DM fitting procedure needs a predefined DM model to work, instead the gravitational torques method does not depend on any DM model. In summary the methodology conceived in this article to obtain the semi-axes of the supposed DM triaxial spheroid seems a valid and reliable tool, that can be used as a stand-alone reasonable alternative to the gravitational torques strategy, or at least as a comparative approach, as also confirmed by the synthetic data experiments performed in section 7.1, and, by the contrast with the findings of other authors of section 7.2.

9 CONCLUSIONS

In the foremost part of this study we extend the methodological approach of RP18, through the diagonalization of a 3SSM without zeros, providing a general solution of the Poisson equation to obtain a relation for the gravitational potential suitable to describe several different mass distributions, and ascertaining relations for the semi-axes of a triaxial spheroid expressed as ratios of the DM models masses and scale radii, and the corresponding volume densities. In the second part of the present work we apply the results of the first part, to analyse the DM and total mass amount of UGC 8490 and UGC 9753, in particular to determine the inner and overall DM mass distribution of the two galaxies, by means of the fits to their DM RCs. The validation of the fitting results is accomplished through the computation of the gravitational torques exercised by the DM haloes of UGC 8490 and UGC 9753 on their respective baryonic constituents, through mock data trials, and the comparison with other research works in the existing literature. In more details the enumeration of the principal findings is the following:

- The fits to the $H\alpha$ DM RCs of UGC 8490 and UGC 9753 establish a BKT cored and DCN cuspy inner DM distribution for UGC 8490 and UGC 9753, respectively.
- The fits to the HI DM RCs of UGC 8490 and UGC 9753 reveal a DCN cuspy and NFW cuspy inner DM configuration for UGC 8490 and UGC 9753, separately.
- The global DM distributions of UGC 8490 and UGC 9753 are well fitted by oblate spheroids, and this latter result is confirmed by the computation of the DM haloes gravitational torques on the corresponding baryonic components of both galaxies, and the estimation of the semi-axes of the generated perturbations, and also, through the comparison with other studies.

The inner cuspy DM distribution of UGC 8490 and UGC 9753, is concordant with recent works on the subject (see the previous section and the references therein), and indicates the persistence of a long standing problem, still un-

der intense scrutiny, and whose complete solution demands much more observational and theoretical efforts.

ACKNOWLEDGEMENTS

We have made use of the WSRT on the Web Archive. The Westerbork Synthesis Radio Telescope is operated by the Netherlands Institute for Radio Astronomy ASTRON, with support of NWO. The WHISP observation were carried out with the Westerbork Synthesis Radio Telescope, which is operated by the Netherlands Foundation for Research in Astronomy (ASTRON) with financial support from the Netherlands Foundation for Scientific Research (NWO). The WHISP project was carried out at the Kapteyn Astronomical Institute by J. Kamphuis, D. Sijbring and Y. Tang under the supervision of T.S. van Albada, J.M. van der Hulst and R. Sancisi. This publication makes use of data products from the Two Micron All Sky Survey, which is a joint project of the University of Massachusetts and the Infrared Processing and Analysis Center/California Institute of Technology, funded by the National Aeronautics and Space Administration and the National Science Foundation. We acknowledge the usage of the HyperLeda database (<http://leda.univ-lyon1.fr>). STSDAS and PyRAF are products of the Space Telescope Science Institute, which is operated by AURA for NASA. IRAF is distributed by the National Optical Astronomy Observatories, which is operated by the Association of Universities for Research in Astronomy, Inc. (AURA) under cooperative agreement with the National Science Foundation. We employ the Kapteyn python package (Terlouw & Vogelaar 2014) to build some of the figures of the present article. This research has made use of the SIMBAD database, operated at CDS, Strasbourg, France (Wenger et al. 2000), "The SIMBAD astronomical database", Wenger et al. This research has made use of the NASA/IPAC Extragalactic Database (NED), which is operated by the Jet Propulsion Laboratory, California Institute of Technology, under contract with the National Aeronautics and Space Administration. The IllustrisTNG simulations were undertaken with compute time awarded by the Gauss Centre for Supercomputing (GCS) under GCS Large-Scale Projects GCS-ILLU and GCS-DWAR on the GCS share of the supercomputer Hazel Hen at the High Performance Computing Center Stuttgart (HLRS), as well as on the machines of the Max Planck Computing and Data Facility (MPCDF) in Garching, Germany. This research made use of Astropy, a community-developed core Python package for Astronomy (Astropy Collaboration et al. 2018, 2013). This research made use of matplotlib, a Python library for publication quality graphics (Hunter 2007). This research made use of NumPy (Van Der Walt et al. 2011). This research made use of SciPy (Virtanen et al. 2020). The author would like to express his gratitude to Dr. Paola Marziani, for the careful reading of the present manuscript.

DATA AVAILABILITY

No new data were generated or analysed in support of this research.

REFERENCES

- Allaert F., Gentile G., Baes M., 2017, *A&A*, **605**, A55
- Aramanovich I. G., Guter R. S., Lyusternik L. A., Raukhvarger I. L., Skanavi M. I., Yanpolskii A. R., 1961, *Mathematical Analysis. Differentiation and Integration*. 1th ed.. Pergamon Press
- Arfken G. B., Weber H. J., 2005, *Mathematical methods for physicists* 6th ed.. Elsevier Publishing Services
- Artale M. C., Pedrosa S. E., Tissera P. B., Cataldi P., Di Cintio A., 2019, *A&A*, **622**, A197
- Astropy Collaboration et al., 2013, *A&A*, **558**, A33
- Astropy Collaboration et al., 2018, *AJ*, **156**, 123
- Babcock H. W., 1939, *Lick Observatory Bulletin*, **498**, 41
- Bekki K., Freeman K. C., 2002, *ApJL*, **574**, L21
- Benítez-Llambay A., Frenk C. S., Ludlow A. D., Navarro J. F., 2019, *MNRAS*, **488**, 2387
- Bertin E., Arnouts S., 1996, *A&AS*, **117**, 393
- Binney J., Tremaine S., 2008, *Galactic Dynamics: Second Edition*. Princeton University Press
- Blais-Ouellette S., Amram P., Carignan C., 2001, *AJ*, **121**, 1952
- Blais-Ouellette S., Amram P., Carignan C., Swaters R., 2004, *A&A*, **420**, 147
- de Blok W. J. G., 2018, *Nature Astronomy*, **2**, 615
- de Blok W. J. G., Walter F., Brinks E., Trachternach C., Oh S. H., Kennicutt R. C. J., 2008, *AJ*, **136**, 2648
- Brainerd T. G., Yamamoto M., 2019, *MNRAS*, **489**, 459
- Brandt J. C., 1960, *ApJ*, **131**, 293
- Brun R., Rademakers F., 1997, in *ROOT - An Object Oriented Data Analysis Framework*. Proceedings AIHENP'96 Workshop, Lausanne, Sep. 1996, Nucl. Inst. and Meth. in Phys. Res. A **389** (1997) pp 81-86. See also <http://root.cern.ch/>
- Bryan S. E., Kay S. T., Duffy A. R., Schaye J., Dalla Vecchia C., Booth C. M., 2013, *MNRAS*, **429**, 3316
- Burbidge E. M., Burbidge G. R., Prendergast K. H., 1959, *ApJ*, **130**, 739
- Burkert A., 1995, *ApJ*, **447**, L25
- Burstein D., Rubin V. C., 1985, *ApJ*, **297**, 423
- Burstein D., Rubin V. C., Ford W. K. J., Whitmore B. C., 1986, *ApJ*, **305**, L11
- Buta R. J., et al., 2015, *ApJS*, **217**, 32
- Chemin L., de Blok W. J. G., Mamon G. A., 2011, *AJ*, **142**, 109
- Chua K. T. E., Pillepich A., Vogelsberger M., Hernquist L., 2019, *MNRAS*, **484**, 476
- Ciotti L., Bertin G., 1999, *A&A*, **352**, 447
- Di Cintio A., Brook C. B., Dutton A. A., Macciò A. V., Stinson G. S., Knebe A., 2014, *MNRAS*, **441**, 2986
- Di Teodoro E. M., Fraternali F., 2014, *A&A*, **567**, A68
- Drakos N. E., Taylor J. E., Berrouet A., Robotham A. S. G., Power C., 2019, *MNRAS*, **487**, 993
- Dutton A. A., Macciò A. V., 2014, *MNRAS*, **441**, 3359
- Einasto J., 1965, *Trudy Astrofizicheskogo Instituta Alma-Ata*, **5**, 87
- Forbes D. A., 1992, *Astronomy and Astrophysics Supplement Series*, **92**, 583
- García-Burillo S., Combes F., Schinnerer E., Boone F., Hunt L. K., 2005, *A&A*, **441**, 1011
- Giocoli C., Tormen G., Sheth R. K., van den Bosch F. C., 2010, *MNRAS*, **404**, 502
- Ho L. C., Filippenko A. V., Sargent W. L. W., 1997, *ApJS*, **112**, 315
- Hu S., Sijacki D., 2016, *MNRAS*, **461**, 2789
- Hubble E. P., 1929, *ApJ*, **69**, 103
- Hunter J. D., 2007, *Computing In Science & Engineering*, **9**, 90
- Karachentsev I. D., et al., 2003, *A&A*, **398**, 467
- Karukes E. V., Salucci P., Gentile G., 2015, *A&A*, **578**, A13
- Kent S. M., 1987, *AJ*, **93**, 816
- Korsaga M., Carignan C., Amram P., Epinat B., Jarrett T. H.,

2018, *MNRAS*, **478**, 50

Kravtsov A. V., Klypin A. A., Bullock J. S., Primack J. R., 1998, *ApJ*, **502**, 48

Kuzio de Naray R., McGaugh S. S., Mihos J. C., 2009, *ApJ*, **692**, 1321

Lange J. U., van den Bosch F. C., Hearin A., Campbell D., Zentner A. R., Villarreal A., Mao Y.-Y., 2018, *MNRAS*, **473**, 2830

Li P., Lelli F., McGaugh S., Schombert J., 2018, *A&A*, **615**, A3

Li P., Lelli F., McGaugh S., Schombert J., 2020, *ApJS*, **247**, 31

MacArthur L. A., Courteau S., Holtzman J. A., 2003, *ApJ*, **582**, 689

Makarov D., Prugniel P., Terekhova N., Courtois H., Vauglin I., 2014, *A&A*, **570**, A13

Marinacci F., et al., 2018, *MNRAS*, **480**, 5113

McQuinn K. B. W., Lelli F., Skillman E. D., Dolphin A. E., McGaugh S. S., Williams B. F., 2015, *MNRAS*, **450**, 3886

Naiman J. P., et al., 2018, *MNRAS*, **477**, 1206

Navarro J. F., Frenk C. S., White S. D. M., 1996, *ApJ*, **462**, 563

Navarro J. F., et al., 2004, *MNRAS*, **349**, 1039

Nelson D., et al., 2018, *MNRAS*, **475**, 624

Nelson D., et al., 2019, *Computational Astrophysics and Cosmology*, **6**, 2

Oh S.-H., de Blok W. J. G., Walter F., Brinks E., Kennicutt Robert C. J., 2008, *AJ*, **136**, 2761

Oman K. A., et al., 2015, *MNRAS*, **452**, 3650

Persic M., Salucci P., 1990, *ApJ*, **355**, 44

Persic M., Salucci P., Stel F., 1996, *MNRAS*, **281**, 27

Pillepich A., et al., 2018, *MNRAS*, **475**, 648

Plana H., Amram P., Mendes de Oliveira C., Balkowski C., 2010, *AJ*, **139**, 1

Putko J., Sánchez Almeida J., Muñoz-Tuñón C., Asensio Ramos A., Elmegreen B. G., Elmegreen D. M., 2019, *ApJ*, **883**, 10

Relatores N. C., et al., 2019, *ApJ*, **887**, 94

Ren T., Kwa A., Kaplinghat M., Yu H.-B., 2019, *Physical Review X*, **9**, 031020

Repetto P., Martínez-García E. E., Rosado M., Gabbasov R., 2015, *MNRAS*, **451**, 353

Repetto P., Martínez-García E. E., Rosado M., Gabbasov R., 2018, *MNRAS*, **477**, 678

Rubin V. C., Ford W. K. J., Thonnard N., 1978, *ApJ*, **225**, L107

Rubin V. C., Burstein D., Ford W. K. J., Thonnard N., 1985, *ApJ*, **289**, 81

Salucci P., Nesti F., Gentile G., Frigerio Martins C., 2010, *A&A*, **523**, A83

Santos-Santos I. M. E., et al., 2019, arXiv e-prints, [p. arXiv:1911.09116](https://arxiv.org/abs/1911.09116)

Schoenmakers R. H. M., Franx M., de Zeeuw P. T., 1997, *MNRAS*, **292**, 349

Sengupta C., Balasubramanyam R., 2006, *MNRAS*, **369**, 360

Sicotte V., Carignan C., 1997, *AJ*, **113**, 609

Skrutskie M. F., Cutri R. M., Stiening R., Weinberg 2006, *AJ*, **131**, 1163

Spano M., Marcelin M., Amram P., Carignan C., Epinat B., Hernandez O., 2008, *MNRAS*, **383**, 297

Springel V., et al., 2008, *MNRAS*, **391**, 1685

Springel V., et al., 2018, *MNRAS*, **475**, 676

Stadel J., Potter D., Moore B., Diemand J., Madau P., Zemp M., Kuhlen M., Quilis V., 2009, *MNRAS*, **398**, L21

Swaters R. A., van Albada T. S., van der Hulst J. M., Sancisi R., 2002, *A&A*, **390**, 829

Swaters R. A., Madore B. F., van den Bosch F. C., Balcells M., 2003, *ApJ*, **583**, 732

Takamiya T., Sofue Y., 2000, *ApJ*, **534**, 670

Terlouw J. P., Vogelaar M. G. R., 2014, Kapteyn Package, version 3.0. Kapteyn Astronomical Institute, Groningen

Tissera P. B., White S. D. M., Pedrosa S., Scannapieco C., 2010, *MNRAS*, **406**, 922

Touma J., Tremaine S., 1997, *MNRAS*, **292**, 905

Van Der Walt S., Colbert S. C., Varoquaux G., 2011, Computing in Science & Engineering, 13, 22

Velliscig M., et al., 2015, *MNRAS*, **453**, 721

Virtanen P., Gommers R., Oliphant T. E., Haberland M., Reddy T., Cournapeau D., Burovski E., Peterson 2020, *Nature Methods*, **17**, 261

Vogelaar M. G. R., Terlouw J. P., 2001, The Evolution of GIPSY—or the Survival of an Image Processing System. Harnden, F. R., Jr. and Primini, Frances A. and Payne, Harry E., p. 358

Wenger M., et al., 2000, *A&AS*, **143**, 9

Wyse A. B., Mayall N. U., 1942, *ApJ*, **95**, 24

Yeh L.-C., Jiang I.-G., 2018, *Research in Astronomy and Astrophysics*, **18**, 153

van Dokkum P., et al., 2019, *ApJ*, **880**, 91

van der Hulst J. M., Terlouw J. P., Begeman K. G., Zwitser W., Roelfsema P. R., 1992, The Groningen Image Processing System, GIPSY. Worrall, Diana M. and Biemesderfer, Chris and Barnes, Jeannette, p. 131

APPENDIX A: DIAGONALIZATION OF A 3SSM WITHOUT ZERO ELEMENTS

In the present addendum we reduce to diagonal form a 3SSM, whose entries are all different from zero. The latter result is an essential instrument to orthogonalise systems of curvilinear coordinates that are not orthogonal. Primarily we introduce the matrices M_{ml} and M_{ll} , that represent the 3SSM and the matrix resulting from the diagonalization of the 3SSM, respectively. The definitions of the 3SSM, the resultant diagonal matrix, their characteristic polynomials and the system of equations generated from the equalities among the coefficients of the particular characteristic polynomials of M_{ml} and M_{ll} are displayed below.

$$M_{ml} = \begin{pmatrix} v_{11} & v_{12} & v_{13} \\ v_{21} & v_{22} & v_{23} \\ v_{31} & v_{32} & v_{33} \end{pmatrix} \quad M_{ll} = \begin{pmatrix} V_{11} & 0 & 0 \\ 0 & V_{22} & 0 \\ 0 & 0 & V_{33} \end{pmatrix} \quad (A1)$$

$$\begin{aligned} p1(q) = & q^3 - q^2(v_{11} + v_{22} + v_{33}) + \\ & + q(v_{11}v_{22} + v_{11}v_{33} + v_{22}v_{33} - v_{12}^2 - v_{13}^2 - v_{23}^2) + \\ & - (v_{11}v_{22}v_{33} + 2v_{12}v_{13}v_{23} - v_{12}^2v_{33} - v_{13}^2v_{22} + \\ & - v_{23}^2v_{11}) = 0 \end{aligned} \quad (A2)$$

$$\begin{aligned} p2(q) = & q^3 - q^2(V_{11} + V_{22} + V_{33}) + \\ & + q(V_{11}V_{22} + V_{11}V_{33} + V_{22}V_{33}) - V_{11}V_{22}V_{33} = 0 \end{aligned} \quad (A3)$$

$$\begin{aligned} V_{11} + V_{22} + V_{33} = & v_{11} + v_{22} + v_{33} \\ V_{11}V_{22} + V_{11}V_{33} + V_{22}V_{33} = & v_{11}v_{22} + v_{11}v_{33} + v_{22}v_{33} + \\ & - v_{12}^2 - v_{13}^2 - v_{23}^2 \\ V_{11}V_{22}V_{33} = & v_{11}v_{22}v_{33} + 2v_{12}v_{13}v_{23} - v_{12}^2v_{33} - v_{13}^2v_{22} + \\ & - v_{23}^2v_{11}. \end{aligned} \quad (A4)$$

The system of equations above can be solved considering 9 quadratic equations, that have as unknown quantities the entries of M_{ll} arranged according to all possible permutations of their respective indices. In particular, we indicate

the diagonal matrix elements as V_{ii}, V_{jj}, V_{kk} , where the indices i, j, k cycle from 1 to 3 according to different combination, and cannot be equal simultaneously. In detail, the solution strategy equates the quantities $V_{jj} + V_{kk}$ from the first equation of the system above with the identical binomial sums extracted from the second equation of the same system. The principal hypotheses to apply this procedure are that $V_{jj}V_{kk} = v_{jj}v_{kk} - v_{jk}^2$, (eq. a), and as a consequence that $V_{jj}V_{ii} + V_{ii}V_{kk} = v_{jj}v_{ii} + v_{ii}v_{kk} - v_{ji}^2 - v_{ik}^2$, (eq. b), as we readily verify once obtained the three diagonal matrix terms. This methodology determines three quadratic equations in the variable V_{ii} that we report below:

$$V_{ii}^2 - V_{ii} [\text{Tr}(M_{ml})] + v_{jj}v_{ii} + v_{ii}v_{kk} - v_{ji}^2 - v_{ik}^2 = 0. \quad (\text{A5})$$

The solutions to equations (A5) are the relations (A6), that we specify below, together with the corresponding discriminants:

$$V_{ii}^{(+,-)} = \left[\frac{\text{Tr}(M_{ml}) \pm \Delta^{(i)}}{2} \right]$$

$$\Delta^{(i)} = \sqrt{[v_{kk} + v_{jj} - v_{ii}]^2 + 4(v_{ji}^2 + v_{ik}^2)}. \quad (\text{A6})$$

The remaining diagonal terms V_{kk} and V_{jj} are obtained solving the system of equations formed by the relations (a) and (b), and, replacing V_{ii} with the relations of equations (A6), to determine six quadratic equations, three in the variables V_{kk} , and other three in the variable V_{jj} . The most important details are provided below:

$$V_{kk} = [\text{Tr}(M_{ml}) - V_{ii}^{(+,-)} - V_{jj}] \Rightarrow V_{kk} = V_{ii}^{(-,+)} - V_{jj} \Rightarrow$$

$$V_{kk}^2 - V_{kk} [V_{ii}^{(-,+)}] + (v_{jj}v_{kk} - v_{jk}^2) = 0. \quad (\text{A7})$$

The exact solutions to the three quadratic equations for V_{kk} are the following:

$$V_{kk}^{(+,-)} = \frac{1}{2} \left\{ V_{ii}^{(-,+)} \pm \Delta_1^{(i)} \right\}$$

$$\Delta_1^{(i)} = \sqrt{[V_{ii}^{(-,+)}]^2 - 4(v_{jj}v_{kk} - v_{jk}^2)}. \quad (\text{A8})$$

The three solution for V_{jj} are readily obtained from the sums $V_{jj} + V_{kk}^{(+,-)}$ according to the ensuing description:

$$V_{jj}^{(-,+)} = V_{ii}^{(-,+)} - V_{kk}^{(+,-)} = \frac{1}{2} \left\{ V_{ii}^{(-,+)} \mp \Delta_1^{(i)} \right\}. \quad (\text{A9})$$

The verification of the initial assumptions about the products $V_{jj}V_{kk}$ and the relations $V_{ii}(V_{jj} + V_{kk})$ are provided by the next expressions:

$$V_{jj}^{(-,+)}V_{kk}^{(+,-)} = \frac{1}{4} \left\{ [V_{ii}^{(-,+)}]^2 - [\Delta_1^{(i)}]^2 \right\} =$$

$$= v_{jj}v_{kk} - v_{jk}^2$$

$$V_{ii}^{(+,-)}(V_{jj}^{(-,+)} + V_{kk}^{(+,-)}) = V_{ii}^{(+,-)}V_{ii}^{(-,+)} =$$

$$\frac{1}{4} \left\{ [\text{Tr}(M_{ml})]^2 - [\Delta^{(i)}]^2 \right\} = v_{ii}(v_{jj} + v_{kk}) - v_{ji}^2 - v_{ik}^2. \quad (\text{A10})$$

The first two relations of the system expressed by equation (A4) could be quickly verified employing the nine solutions for the diagonal matrix entries V_{jj} , V_{ii} and V_{kk} . The sum of the fourth and second relation of equation (A10) constitutes the second row of the system (A4). The first equation of the same system can be obtained immediately through the sum of the solutions $V_{jj}^{(-,+)}$, $V_{ii}^{(+,-)}$ and $V_{kk}^{(+,-)}$. The third equation is a consequence of the fact that the diagonal matrix is and endomorphism of the 3SSM and therefore the respective determinants have to be equal. The latter property is identical to the equality between the characteristic polynomials with null independent variable, as one promptly realises equating equations (A2) and (A3) with $q = 0$. The procedure to determine some special instances of the nine solutions obtained in the current addendum is delineated at the end of section (2.1).

APPENDIX B: DETERMINATION OF AN INTEGRAL SOLUTION OF THE POISSON EQUATION

In this addendum we derive an integral solution of the Laplace and Poisson equations, in order to determine a relation of the 3D gravitational potential as a function of the entries of the diagonal metric tensor matrix. The resultant expression of the gravitational potential is suitable to represent several different mass density distributions, defined either through orthogonal systems of coordinates, or non orthogonal systems of coordinates, that can be converted to orthogonal form, by means of the diagonalization of the metric tensor matrix that defines the initial non orthogonal system of curvilinear coordinates. Primarily we accomplish the solution of the homogeneous part of the Poisson equation, i.e. the Laplace equation. The most important steps of that result are delineated below. The Laplace equation expressed as a function of the diagonal elements of the metric tensor matrix reads (Arfken & Weber 2005):

$$\frac{1}{\sqrt{V}} \left[\sum_{s=1}^3 \frac{\partial}{\partial u_s} \left(\sqrt{V} V^{ss} \frac{\partial \phi_s(u_1, u_2, u_3)}{\partial u_s} \right) \right] = 0 \quad (\text{B1})$$

The three solutions are obtained setting each term in the sum equal to zero, and are detailed below:

$$\frac{\partial \phi_{(t,p,q)}(u_1, u_2, u_3)}{\partial u_{(t,p,q)}} =$$

$$= \left[C_{st} \sqrt{\frac{V_{tt}}{V_{pp}V_{qq}}}, C_{sp} \sqrt{\frac{V_{pp}}{V_{tt}V_{qq}}}, C_{sq} \sqrt{\frac{V_{qq}}{V_{tt}V_{pp}}} \right] \quad (\text{B2})$$

where the variables (t, p, q) take the values 1, 2, 3, respectively, and the quantity $C_{s(t,p,q)}$ are constants whose units have to be determined for each specific instance separately. The non homogeneous equation i.e. the Poisson equation, can be expressed in the following manner:

$$\frac{1}{\sqrt{V}} \left[\sum_{s=1}^3 \frac{\partial}{\partial u_s} \left(\sqrt{V} V^{ss} \frac{\partial \phi_s(u_1, u_2, u_3)}{\partial u_s} \right) \right] = 4\pi G \left[\sum_{s=1}^3 \rho_s(u_1, u_2, u_3) \right] \quad (\text{B3})$$

The solution strategy expresses the volume densities as the partial derivative of the corresponding mass densities to transform the Poisson equation in a homogeneous equation that can be solved equating each terms to zero. The volume densities can be related to the mass densities in the following way:

$$\rho_s(u_1, u_2, u_3) = \frac{1}{\sqrt{V}} \frac{\partial^3 M_s(u_1, u_2, u_3)}{\partial u_1 \partial u_2 \partial u_3} \quad (\text{B4})$$

replacing the volume densities in equation (B3), by means of the latter expressions, we obtain the ensuing relations:

$$\sum_{s=1}^3 \frac{\partial}{\partial u_s} \left[\sqrt{V} V^{ss} \frac{\partial \phi_s(u_1, u_2, u_3)}{\partial u_s} + \frac{1}{\sqrt{V}} \frac{\partial^3 M_s(u_1, u_2, u_3)}{\partial u_1 \partial u_2 \partial u_3} \right] = 0 \quad (\text{B5})$$

In the above expression, the term within square brackets, is constant and consequently we obtain the following solutions of the Poisson equation:

$$\frac{\partial \phi_s(u_1, u_2, u_3)}{\partial u_s} = \frac{4\pi G}{\sqrt{V} V^{ss}} \frac{\partial^2 M_s(u_1, u_2, u_3)}{\partial u_p \partial u_q} + \frac{C_{s(t,p,q)}}{\sqrt{V} V^{ss}} \quad (\text{B6})$$

The constants $C_{s(t,p,q)}$ are identical to those encountered for the Laplace equation, the quantities $\left[\sqrt{V} V^{ss} \right]^{-1}$ are equal to those reported in equation (B2), and the term involving the partial derivatives of the 3D mass density function can be expressed as follows:

$$\frac{\partial^2 M_s(u_1, u_2, u_3)}{\partial u_p \partial u_q} = \int_0^{u_s} \rho_s(v_1, v_2, v_3) \sqrt{V} dv_s \quad (\text{B7})$$

introducing equation (B7) into equation (B6), we obtain the following solutions of the Poisson equation:

$$\frac{\partial \phi_s(u_1, u_2, u_3)}{\partial u_s} = \frac{4\pi G}{\sqrt{V} V^{ss}} \int_0^{u_s} \rho_s(v_1, v_2, v_3) \sqrt{V} dv_s + \frac{C_{s(t,p,q)}}{\sqrt{V} V^{ss}} \quad (\text{B8})$$

The precise definition of the quantities $\left[\sqrt{V} V^{ss} \right]^{-1}$ is the following:

$$\frac{1}{\sqrt{V} V^{ss}} = \left[\sqrt{\frac{V_{tt}}{V_{pp} V_{qq}}}, \sqrt{\frac{V_{pp}}{V_{tt} V_{qq}}}, \sqrt{\frac{V_{qq}}{V_{tt} V_{pp}}} \right] \quad (\text{B9})$$

The variables (t, p, q) are identical to those defined in equation (B2), and the solutions expressed by equation (B8), represent the first order partial derivatives of the gravitational potential of a given mass distribution. The volume density points that constitute that mass distribution are defined through a set of orthogonal curvilinear coordinates (u_1, u_2, u_3), nonetheless the solutions (B8) can be applied also to non orthogonal system of coordinates, once reduced to orthogonal form by means of the diagonalization of the metric tensor matrix that describes the original system of non orthogonal curvilinear coordinates. In section (3), we consider the solution determined by setting $s = 1$, in equation (B8), that specific relation is fundamental to address the particular question analysed in the current work.

APPENDIX C: METRIC TENSOR MATRIX ELEMENTS FOR A TRIAXIAL SPHEROIDAL GEOMETRY

We consider the correspondence between the rectangular coordinates $x_i = (x_1, x_2, x_3)$ and the triaxial spheroidal curvilinear coordinates $v_i = (v_1, v_2, v_3)$, expressed by the following relations:

$$\begin{aligned} x_1 &= v_1 a_1 \cos v_2 \sin v_3 \\ x_2 &= v_1 a_2 \sin v_2 \sin v_3 \\ x_3 &= v_1 a_3 \cos v_3 \end{aligned} \quad (\text{C1})$$

where $v_1 = \left[\sum_{i=1}^3 \frac{x_i^2}{a_i^2} \right]^{\frac{1}{2}}$ represents the radius of the triaxial spheroid and a_1, a_2 and a_3 are the semi-axes, parallel to the x_1, x_2 and x_3 axes, respectively. The azimuthal and zenithal coordinates are v_2 and v_3 , separately. The metric tensor matrix entries are determined from equation (C1), their definitions (e.g. Aramanovich et al. 1961) are reported in equation (C2), whereas their expressions are described in equation (C3):

$$v_{jj} = \sum_{l=1}^3 \left[\frac{\partial x_l}{\partial v_j} \right]^2 \quad j = 1, 2, 3 \quad v_{mk} = \sum_{l=1}^3 \left[\frac{\partial x_l}{\partial v_m} \frac{\partial x_l}{\partial v_k} \right] \quad (\text{C2})$$

where the integers m and k assume the values (1, 1, 2) and (2, 3, 3) respectively. The relations of the elements of the metric tensor matrix, in triaxial spheroidal curvilinear coordinates, are reported below:

$$\begin{aligned} v_{11} &= \sin^2 v_3 [a_1^2 \cos^2 v_2 + a_2^2 \sin^2 v_2] + a_3^2 \cos^2 v_3 \\ v_{22} &= v_1^2 \sin^2 v_3 [a_1^2 \sin^2 v_2 + a_2^2 \cos^2 v_2] \\ v_{33} &= v_1^2 \{ \cos^2 v_3 [a_1^2 \cos^2 v_2 + a_2^2 \sin^2 v_2] + a_3^2 \sin^2 v_3 \} \\ v_{12} &= v_1 \cos v_2 \sin v_2 \sin^2 v_3 [a_2^2 - a_1^2] \\ v_{13} &= v_1 \cos v_3 \sin v_3 [a_1^2 \cos^2 v_2 + a_2^2 \sin^2 v_2 - a_3^2] \\ v_{23} &= v_1^2 \cos v_2 \sin v_2 \cos v_3 \sin v_3 [a_2^2 - a_1^2]. \end{aligned} \quad (\text{C3})$$

The quantity \sqrt{V} is determined through the determinant of the Jacobian matrix, taking advantage of the equality among the determinant of the metric tensor matrix and the square of the Jacobian determinant.

APPENDIX D: TRIAXIAL SPHEROID SEMI-AXES CONSTRAINTS

This addendum is dedicated to the derivation of the semi-axes relations of a triaxial spheroidal mass density configuration that it is supposed to describe appropriately the DM haloes of UGC 8490 and UGC 9753. It is demonstrated that the semi-axes of the hypothesised triaxial spheroid can be expressed as constant quotients of the resultant DM fitting parameters, such as, for instance, the DM halo masses, scale radii, and the corresponding spatial densities. First of all we obtain the product of the three semi-axes $a_1 a_2 a_3$, from the definition of the radial mass density, of an hypothetical triaxial spheroid:

$$a_1 a_2 a_3 = \frac{1}{4\pi v_1^2 \rho_E(v_1)} \frac{dM_E(v_1)}{dv_1} \quad (\text{D1})$$

where the quantity $\rho_E(v_1)$ represents the radial volume density of the triaxial spheroid. In this appendix we solely perform the detailed derivation of the semi-axes product $a_1 a_2$, that involve the equatorial ellipse, since the determination of the products, $a_1 a_3$ and $a_2 a_3$, that correspond to the two ellipses perpendicular to the equatorial ellipse, is based on identical arguments. The product of the semi-axes of the equatorial ellipse $a_1 a_2$ is obtained from the definition of its surface mass density in the following way:

$$\begin{aligned} \frac{dM_{EE}(s_1)}{ds_1} &= 2\pi a_1 a_2 \Sigma_{EE}(s_1) s_1 \quad s_1 = v_1 \sin v_3 \Rightarrow \\ \frac{dM_{EE}(s_1)}{dv_1} &= 2\pi a_1 a_2 \Sigma_{EE}(s_1) v_1 \sin^2 v_3 \end{aligned} \quad (\text{D2})$$

The equatorial surface density $\Sigma_{EE}(s_1)$ can be expressed as a function of the triaxial spheroid radial mass density $M_E(v_1)$, through the surface density definition and equation (D1). The resultant expression of the equatorial surface density is the ensuing:

$$\begin{aligned} \Sigma_{EE}(s_1) &= 2 \int_0^{x_{3m}} \rho_E(v_1) dx_3 \quad x_3 = v_1 a_3 \cos v_3 \Rightarrow \\ \Sigma_{EE}(s_1) &= \frac{\cos v_3}{2\pi a_1 a_2} \int_0^{x_{3m}} \frac{1}{v_1^2} \frac{dM_E(v_1)}{dv_1} dv_1 \end{aligned} \quad (\text{D3})$$

The quantity x_{3m} defines the maximum extension of the x_3 coordinates. Introducing equation (D3) into equation (D2), we determine the following expression for the first derivative of the equatorial mass surface density, and for the product $a_1 a_2$:

$$\begin{aligned} \frac{dM_{EE}(s_1)}{dv_1} &= v_1 \sin^2 v_3 \cos v_3 \int_0^{x_{3m}} \frac{1}{v_1^2} \frac{dM_E(v_1)}{dv_1} dv_1 = \\ &= 2\pi a_1 a_2 \Sigma_{EE}(s_1) v_1 \sin^2 v_3 \Rightarrow a_1 a_2 = \frac{1}{4\pi} \left[\frac{I_{3M}}{I_{3d}} \right] \\ I_{3M} &= \int_0^{x_{3m}} \frac{1}{v_1^2} \frac{dM_E(v_1)}{dv_1} dv_1 \quad I_{3d} = \int_0^{x_{3m}} \rho_E(v_1) dx_3 \end{aligned} \quad (\text{D4})$$

The angular part of the semi-axes relations determined in the present addendum, is computed for constant values of the angles v_3 and v_2 , depending on the considered symmetries within the analysed spheroidal mass distribution, and those constant values are included as part of the integral

ratios $\frac{I_{3M}}{I_{3d}}$, and, the latter observation is valid also for the derivation of the other semi-axes products. The integrals I_{3M} and I_{3d} can be computed analytically, and as a consequence the ratio of the two integrals is a constant without physical units. We perform the integrals calculation elsewhere, however we do not report that computation here, because of its lengthiness. The product $a_1 a_2$, as well as, any other semi-axes products can be expressed by means of the results of the DM fitting parameters, such as, for instance, the DM halo masses, scale radii, and the corresponding volume densities. The determination of the other semi-axes products follows the same line of reasoning, considering the surface mass densities of the two other ellipses orthogonal to the equatorial ellipses, and that contain the semi axes a_2 , a_3 , and a_1 , a_3 , respectively. The three semi-axes products are given by the following expressions:

$$\begin{aligned} a_1 a_2 &= \frac{1}{4\pi} \left[\frac{I_{3M}}{I_{3d}} \right] & a_1 a_3 &= \frac{1}{4\pi} \left[\frac{I_{2M}}{I_{2d}} \right] \\ a_2 a_3 &= \frac{1}{4\pi} \left[\frac{I_{1M}}{I_{1d}} \right] \end{aligned} \quad (\text{D5})$$

The equations (4.1) and (4.2) are obtained from the system of products above, and the precise expressions of the integral ratios, obtained after the integrals computation, are quotients of two masses of different magnitudes to produce constants, whose values are lesser or greater than unity, or even equal to unity, and without any physical dimensions. We employ the semi-axes relations of section (3) to establish the actual mass density configuration of the DM haloes of UGC 8490 and UGC 9753.

This paper has been typeset from a $\text{\TeX}/\text{\LaTeX}$ file prepared by the author.